Authors' response to comments received to manuscript *"Comparing SOA volatility distributions derived from isothermal SOA particle evaporation data and FIGAERO-CIMS measurements"*

We thank both reviewer #1 and reviewer #2 for reviewing our manuscript and for the insightful comments that helped to improve the manuscript. Below we address the comments presented by the reviewers. The comments of the reviewers are **shown in bold,** our answers are shown as normal text, and the changes made to the manuscript are *shown in italic*. To improve readability we have numbered the comments of reviewer #2. All the line numbers given refer to the revised version of the manuscript.

Please note that the parametrization used for calculating effective saturation mass concentration C^* from the desorption temperatures of each PMF factor is different in the revised version of the manuscript than in the ACPD version of the manuscript. The parameterization used in the ACPD version corresponded for a different type of FIGAERO and we have now revised the results using a parametrization applicable for the FIGAERO used in this study. The parametrization used in the revised version results in lower C^* than the parametrization used in the ACPD version with the same desorption temperature input. This correction did not change our main conclusions. However, the new parametrization affects the results discussed in the comments 10 and 15 by the reviewer #2.

Reviewer #1

In this manuscript, Tikkanen et al. compare SOA volatility derived from two different analyses: isothermal evaporation data and PMF applied to FIGAERO-CIMS data.Volatility is a critical property of organic aerosol, and I agree with the authors that the volatility data from FIGAERO-CIMS measurements have been under-utilized. This manuscript focuses on the comparison of the FIGAERO-CIMS PMF volatility data to isothermal evaporation data; the details of the FIGAERO-CIMS PMF volatility analysis are described in another manuscript currently under review (Buchholz et al., 2019 https://www.atmos-chem-phys-discuss.net/acp-2019-926/). It seems to me that this manuscript can only be accepted if Buchholz et al., 2019 is also accepted. I also request that my specific comments below be addressed before publication of this manuscript.

The companion manuscript Buchholz et al. (2019b) is now at the "Editor Final Decision" status after some further minor revisions.

1. The authors use data from previously conducted experiments in which SOA wasformed from alpha-pinene and ozone/OH. By varying experimental conditions, the SOA produced had low, medium or high O:C. Here, the authors only use experiments when the SOA formed had low or medium O:C. This choice is currently not explained or justified in the manuscript. In my opinion, the dataset utilized here is fairly limited,and the analysis would benefit from inclusion of these additional high O:C data. For

Example, overall the authors find that the agreement between the two volatility analysis better for intermediate O:C than for low O:C, and I am curious about the agreement at high O:C.

Answer: The detailed analysis of the high O:C evapogram and particle composition data presented in Buchholz et al., (2019a and 2019b) strongly suggests an important influence of particle phase chemistry for these particles in the wet cases. For example, Buchholz et al., (2019a) show that one of the PMF factors has a significant contribution to the total thermogram in the wet RTC sample (sample taken at the later stages of the evaporation) even though the same factor is virtually non-existing in the fresh sample. This means that compounds were being formed during the isothermal evaporation experiment.

Including the high O:C results in our manuscript would require particle phase chemical reactions to be included in the model. Not enough is known about such reactions and therefore assumptions would need to be made about properties of the reaction products and the extent of the particle phase chemistry happening during the evaporation of the particles. This would lead to considerable uncertainty in the results. In our manuscript we wanted to keep the analysis as simple as possible and therefore elected not to include the more complex high O:C cases to the manuscript. Instead we included only the low and medium O:C cases for which Buchholz et al., (2019a,b) did not observe signs of significant effects from particle phase chemical reactions We have added the following explanation to line 91:

The closer analysis of the high O:C experiments suggest particle phase reactions during the evaporation (Buchholz et al., 2019a,b). To avoid the uncertainty that would arise from unknown particle phase reactions, we chose not to include the high O:C data in our analysis.

2. The main takeaways from the manuscript should be clarified. The authors state in the abstract that “FIGAERO-CIMS measurements analyzed with the PMF method area promising method for inferring organic compounds’ volatility distribution”. The more detailed results point to the method working better under some conditions than others.It would be useful if the authors could make more concrete recommendations for future use of this method (PMF applied to FIGAERO-CIMS data) to obtain information on organic aerosol volatility.

Answer: This comment is also linked to the first and third comment made by reviewer #2 about the discussion part of our manuscript. We have edited the discussion to better frame our findings. Please see our response to Reviewer 2.

Editorial comments: There are several typographical and grammatical errors in the manuscript. I include a list of examples below:

Line 19: “volatility distributions derived the two ways are comparable within reasonable assumption”

Line 233: “and only evaporated th at different conditions”

Line 311: “To investigate the observed discrepancy more detailed”

Line 376: “In this section we compare VDPMF,opt of the fresh samples to VDPMF ofthe RTC sample to study are the two VD comparable.”

Line 521-522: “thermogram data is good estimating the volatility distribution of organic aerosols”

We thank reviewer #1 for pointing out these errors. We have corrected the ones presented here and also other typographical errors we found in the manuscript.

Reviewer #2

Review of acp-2019-927 ”Comparing SOA volatility distributions derived from isothermal SOA particle evaporation data and FIGAERO-CIMS measurements” by Olli-PekkaTikkanen, Angela Buchholz, Arttu Ylisirniö, Siegfried Schobesberger, Annele Virtanen,and Taina Yli-Juuti

This paper describes a study that compared volatility distributions derived from direct evaporation measurements to estimates derived from measurements made using a FIGAERO-CIMS. Given the central role gas-particle partitioning plays in determining the amount of organic aerosol, this is an important topic. The FIGAERO-CIMS provides information on composition as a function of evaporation temperature but it has not been widely evaluated in the context of figuring out volatility distribution of complex aerosols.The paper describes a detailed analysis of previously published, relatively limited set of data – SOA formed from alpha-pinene formed in a oxidation flow reactor at two differentO:C levels (low and medium). They consider low and high relative humidity and two different residence times. The very limited amount of the data is a real limitation to the paper.

1. Major comments/issues that broadly apply to the manuscript –I found the paper to be a super detailed methods paper. It was not clear why it was submitted to ACP and not a journal like AMTD or AST. Based on the way the paper is written now, those journals are a better fit for the manuscript. My feeling is that while the topic of organic aerosol volatility is relevant to ACP this paper seemed is a very narrow and specialized for that journal (to me it read like a physical chemistry methods papers).

Answer: In our manuscript we show that volatility information derived from FIGAERO-CIMS data is in agreement with the volatility information derived from isothermal evaporation experiments. Considering the recent popularity of the FIGAERO-CIMS instrument in laboratory and atmospheric studies, we feel that this finding is of general interest to the ACP audience.

We agree that the presentation of our manuscript is somewhat more technical than the ACP audience may expect. We have edited the discussion part of our manuscript to better frame our findings and balance the text against the technical details of our study.

2. I had a hard time interpreting some the figures (e.g. Figure 2), which were often very detailed and contained many comparisons. For example, do you really need to show the three different VDevap results on Figures 2, 3 and 7 3 given they are basically the same – seems like an SI detail to help the focus the figure on what is important. This results in the paper have a bit of kitchen sink feel.

Answer: Thank you for this suggestion which helped as to clarify the presentation. We have edited the figures and tables the following way:

- We moved the old figures 2, 3, 4, 5, 6 and 7 and tables 2 and 3, which show the VD_{PMF} derived assuming different sample evaporation times to the supplementary material.
    - The new figures 2, 3, 4, 5, 6 and 7 and table 2 show the analysis only at the mean PMF sample evaporation time for the fresh samples (and at minimum PMF sample evaporation time of the RTC samples in figures 4 and 5 and table 2).
    - The old table 2 has been moved entirely to the supplement
    - The captions of the figures 2, 3, 4, 5, 6 and 7 have been edited to describe the new figures better

Due to these changes in the presentation of the figures and tables we have also edited the main text where the figures are described in the results section.

3. A closely related comment to the previous one, while the text described the figures and the results, I found it lacking in discussion of the results were telling us, specifically around this technique. There was too much focus on describing the data versus what the data are telling us about the technique and aerosol volatility. If it is to

be accepted in ACP, I think the paper should be extensively rewritten to make it more accessible and understandable to the ACP audience.

Answer: We have expanded the discussion and conclusion parts of the manuscript to make it more accessible to the general ACP audience and to highlight the main findings. The changes are on lines 505-507, 515-517, 519-523, 540-543, 548-550, 554-557, 562-563.

4. I spent a fair bit of time on the paper and got repeatedly bogged down. E.g. essentially all the tables can easily be moved to SI(maybe keep a very collapsed version of Table 1) because they are likely not of interest to a general ACP reader.

Answer: Please see our answer to comment 2

5. The very limited data set (a handful of conditions) seems like a pretty large limitation.Even for this limited set of data the method appears to not work so well for some conditions (e.g. low O:C in Figure 4b). There was also no discussion of experimental repeatability. There is probably enough data to justifying publication but this limitation of applying to a very narrow set of systems (and potentially overinterpreting the results) needs to be explicitly stated.

Answer: In figure 4 we compare the PMF VD with C* calculated from peak temperature value (T_{max}) of each factor to VD_{evap}. As noted in the results section, the T_{max} value is not adequate for calculating C* when detailed particle dynamics (i.e. evaporation) is modelled. The $VD_{PMF,opt}$ whose C* values are optimized to match the evaporation data is able to capture the evaporation dynamics. The optimization fails only when we assume that the PMF sample represents the evaporating aerosol particles at the start of the fresh sample collection interval Overall the volatilities from FIGAERO-CIMS and isothermal evaporation agree for all our cases as long as the uncertainties in C* are taken into account.

We agree that the data sets available is a narrow one and we have added a note about this limitation in Section 5 lines 540-543

We compared the two methods for obtaining the volatility distribution data for two different particle compositions and two evaporation conditions. The results are promising and suggest that the methods provide volatility distributions that are in agreement. We note that the data set available here is limited and additional investigations on comparing the methods are desirable in the future.

The base case (low O:C a-pinene) has been studied in our lab in five separate measurement campaigns and the isothermal evaporation is the same within measurement error in all cases.

Also in a later campaign, which is not part of this study as the detailed design and settings of the FIGAERO-CIMS were different, we did repeat FIGAERO-CIMS measurements of the same type of aerosol on multiple days. The behavior of the identified PMF factors is the same between the different samples – only the contribution of background and contamination factors changed significantly as the circumstances changed on different days (e.g. switching to a new filter in FIGAERO). We therefore have a good reason to expect that the results presented here were repeatable even though repeated experiments were not included in this study.

6. FIGAERO-CIMS – Given that it uses chemical ionization with iodide as the reagent ion as opposed to electron impact ionization, there are always concerns about mass closure. What fraction of the SOA mass is being detected by the instrument? If a large fraction of the aerosol mass that is not, then that seems like a big problem. This issue needs to be explicitly discussed, including its implications for measuring volatility. More Molecular ions is a big advantage, but not measuring a large fraction of the material seems like a huge limitation as you are trying to draw inferences about the bulk aerosol based on characterizing only a limited fraction of the aerosol.

The I^- anion in an iodide CIMS preferably clusters with molecules which contain hydroxyl-, hydroperoxyl-, carboxyl- or peroxycarboxyl- groups in their structure. Most products of the reaction of a-pinene with OH or O_3 contain two or more of these functional groups. Thus, the majority of them will be detectable with iodide CIMS even though it is more selective than EI. Mass closure studies for a-pinene SOA generated in a smog chamber have been conducted by Isaacman-VanWertz et al., (2017, 2018) comparing FIGAERO-CIMS to measurements with an SMPS (non-mass spectrometry technique) and a High-Resolution time of flight Aerosol Mass Spectrometer (AMS, Aerodyne research Inc., EI ionisation). They observed very good agreement for the detected particle phase carbon if FIGAERO-CIMS was calibrated as they laid out in the Supplement Material to Isaacman-VanWertz et al., (2018). The compounds produced in our study are comparable and thus a similarly good mass closure could be expected if similar sensitivity calibrations had been conducted for our FIGAERO system. However, such calibration is onerous and not available for the datasets at hand. So, by using uncalibrated FIGAERO-CIMS data here, we are implicitly assuming that the sensitivity towards individual compounds is uncorrelated to the compounds' volatility. We are not aware of published research against which to clearly test that assumption, but it appears plausible that less volatile compounds tend to be detected at higher sensitivity (Iyer et al., 2016; Lee et al., 2014). To our aid comes the maximum sensitivity (corresponding to ionization at the kinetic limit), which is obtained, e.g., for most di-carboxylic acids (#C>3). But it is likely that a bias is introduced that shifts FIGAERO-derived SOA compositions towards lower volatility. Indeed, if such a bias was accounted for, it could bring the evapograms modelled using VD_{PMF} closer to the observations, as in particular the initial (fast) evaporation of relatively volatile material may be systematically underestimated when relying on (uncalibrated) FIGAERO data [Note that such bias would less clearly apply to observed desorption signals that are due to thermal decomposition, so, e.g., PMF factors associated with decomposition would still lead to high estimates when their T_{max} is translated to C* (i.e. opposite bias, towards higher volatility), as discussed in Section 3.1.]

We have added the following to the revised version of the manuscript to lines 113-116 to clarify:

Previous studies using FIGAERO-CIMS with iodide as the reagent ion found 50% or better mass closure compared to more established methods of quantifying OA mass (albeit with high uncertainties; (Isaacman-VanWertz et al., 2017; Lopez-Hilfiker et al., 2016). Therefore, it appears that the bulk of reaction products expected from a-pinene oxidation contains the functional groups required for detection by our FIGAERO-CIMS.

And to lines 197-202:

One more potential source of bias is our implicit assumption of a constant sensitivity of the CIMS towards all compounds, which follows from the lack of calibration measurements for our datasets (which indeed is a challenging endeavour; e.g., Isaacman-VanWertz et al., (2018)). It is plausible that less volatile compounds tend to be detected at higher sensitivity (Iyer et al., 2016; Lee et al., 2014), up to a kinetic limit sensitivity. Consequently, a volatility distribution derived from FIGAERO-CIMS thermograms may be biased towards lower volatility (C^* bins), at least for compositions not associated with thermal decomposition.

7. A closely related FIGAERO-CIMS concern – The FIGAERO only ramps to 200 oC (line200). This is likely much too low to evaporate all of the SOA. Can the authors estimate what fraction of mass is evaporated? Do they account for that in any way? This issue needs to explicitly addressed in manuscript.

Answer: As described in the reply to the previous comments, with appropriate sensitivity calibrations, the FIGAERO instrument ramping up to 200 °C gave mass closure with other instruments.

Our (as well as other's, e.g. Mohr et al., 2018) C* calibration suggests that at 200 °C the corresponding C* value is ~10^{-14} µg m^{-3}, meaning compounds with this C* value will desorb at that temperature. This means that the recently defined class of ultra low volatility compounds (ULVOC, Schervish and Donahue, 2020) starting from C* values of $10^{-8.5}$ µg m^{-3} would still be detected. Additionally, one has to keep in mind that many of these E/ULVOC, especially dimers, will decompose at temperatures below their theoretical desorption temperature. The thermal decomposition products will have a much higher volatility and are detected as such. Most of the compounds assigned to the D-type factors are products of such decomposition. This is discussed in section 3.1.

8. Uniqueness of fit – The paper takes a very empirical approach of fitting data to extract volatility distributions. That is fine and expected given the complexity of the aerosols. However, the number of data points is often quite small, comparable to the

number of free parameters. For example, Figure 4 shows∼7 data points that are fit to determine VDevap. How many free parameters are in the VDevap model?

Line 516 indicates that you are fitting both C* and viscosity parameters – that is a lot of free parameters given the amount of data. The fit is clearly very underconstrained. The result is that there are likely many other solutions are close to the nominally best solution. This is an optimization problem and I suspect that the optimization function looks more like a plateau then a sharp peak therefore (within experimental uncertainty) there are likely many good solutions.

While I gave one example where this occurs, this is a general issue with the paper. For example, I am concerned about the same problem for the FIGAERO PMF approach, because that also have many free parameters. Presumably all of these solutions are reasonably close across the data, but I suspect with diverge as one extrapolates away from the data. This is a major issue with these sorts of empirical approaches. The paper needs to explicitly address this issue.

Answer: Here we address only the optimization done to high RH data. The comment refers also to low RH data which we will address in comment 16 where the optimization to low RH data is brought up again.

In an optimization run the amount of data point is small compared to the number of free parameters. When VD mole fractions are optimized based on only the evapogram data (VD_{evap}) the number of free parameters is equal to the number of VD bins minus 1 as the mole fractions must sum to one. When the C^* values are estimated from the high RH data the number of free parameters is equal to the number of PMF factors. However, in the latter case we are not optimizing a completely unconstrained model to the measurements. The C* values are given constraints from the PMF analysis and our goal is to inspect if it is possible to explain the observed evaporation with these values.

Figure AR1 show how the estimated C^* values are distributed among the 50 independent optimization runs performed for each fresh sample and mean sample evaporation time. The figure show that when the C^* of a factor affects the evaporation dynamics i.e. the minimum and/or maximum value of a factor is inside the red dashed lines the C^* values do not change much between different optimization runs. Note that the spread of values can become wider for a factor when its contribution to the total signal is close to zero (e.g. factor MD1a Fig AR1a or LD1a in Fig AR1b).

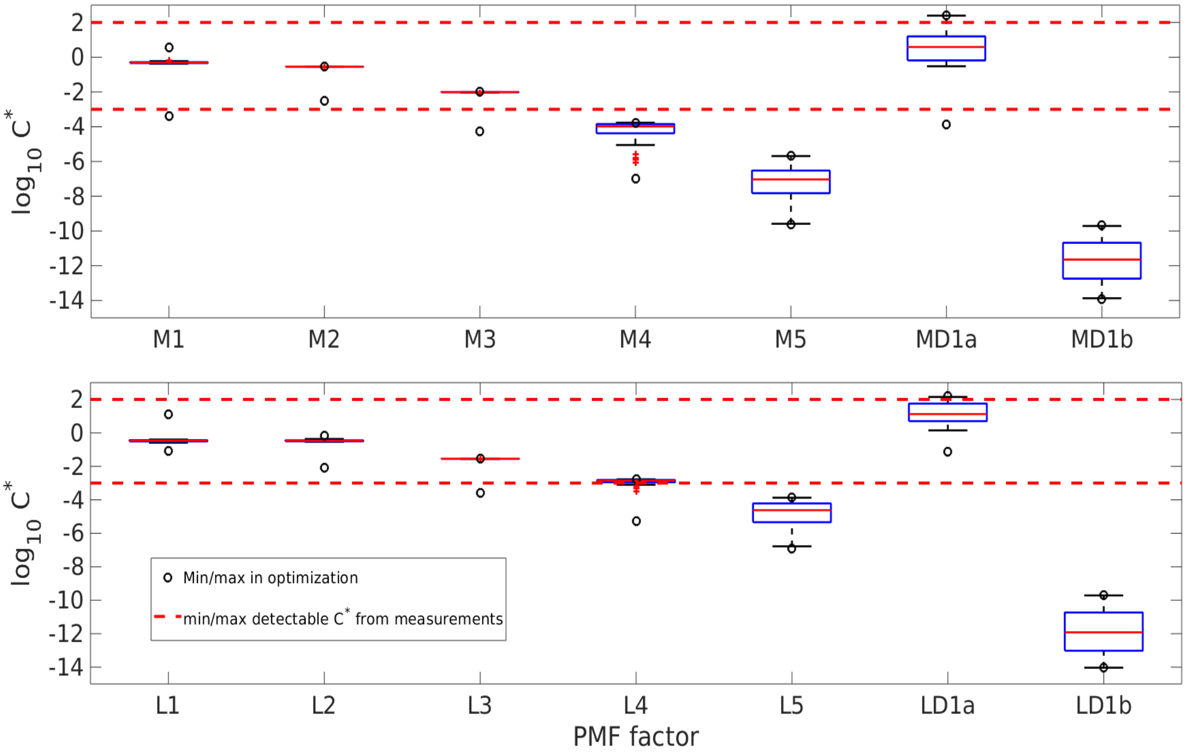

Figure AR1: Box plots showing how the estimated C^* of PMF factors are distributed in 50 independent optimization runs of high RH fresh samples. a) medium O:C mean sample evaporation time b) low O:C mean sample evaporation time Black circles show the minimum and maximum possible value allowed in the optimization (based on the thermograms of the PMF factors) and red dashed lines show the minimum and maximum C^* value that can be estimated from the isothermal evaporation measurements.

9. Here are some specific (but not exhaustive) comments (I spent several hours on this review but was unable to sort through all the details, even though I have published a fair bit on the topic of organic aerosol partitioning).

Line 65 – The paper highlights inconsistency between growth and evaporation experiments. Ultimately C* is a thermodynamic property (certainly at the molecular level) so these inconsistencies point to changing aerosol composition or other properties. Some of this sort of framing may be useful. I.e. if the volatility distribution of the aerosol is really changing, then presumably this reflects some other changes in composition that alters the underlying C* values. Alternatively there could be issues with the kinetics of evaporation. The authors are familiar with all these issues but the introduction might be improved with this framing. To me the issue seems more fundamental then measuring a volatility distribution.

Answer: In line 65 we brought up the difference between SOA evaporation and growth measurements to point out that the volatility information derived from experiments depends on the experiment setup. The limitations of the methods raise a need to develop new tools for extracting the volatility information of SOA constituents.

We have modified the text in line 68-73 in the revised version of the manuscript to

However, the experimental setup also defines the range of C^* values that can be estimated from the data. Vaden et al., (2011) and Yli-Juuti et al., (2017) have both shown that the volatility basis sets derived from SOA growth experiments results in too fast SOA evaporation compared to measured evaporation rates when used as input for process models. Possible reasons for such discrepancies include the different C^* ranges to which the SOA growth and SOA evaporation experiments are sensitive and the role of vapor wall losses in SOA growth experiments.

10. Line 327 – "matches better" Based on what quantitative metric? This is one example of a broader issue of providing quantitative metrics of goodness of fit.

Answer: Note that the simulated evapogram curves in Fig. 4 have changed as we corrected the error in the T_{max}-C^* calibration. The evapograms calculated with the VD_{PMF} of the medium O:C RTC sample produce almost equal evapogram as the one calculated with VD_{evap}. We have adjusted the text accordingly. Also, we increased the readability of the figure by showing only the simulations with medium evaporation time for the FIGAERO samples.

The reviewer is correct, that this is a purely qualitative term and whenever suitable one should use objective and mathematically based parameters for such comparisons. But for this specific example we decided to use a qualitative description rather than goodness of fit statistics. We are comparing the overall shape of the simulated and measured evapograms, but for the evapogram curves simulated with RTC VD_{PMF} we have only 1 or 2 measurement points to directly compare to. It is very clear that the evapograms simulated with the fresh VD_{PMF} underestimate the evaporation (too slow evaporation) for medium O:C particles while those using the RTC VD_{PMF} create curves that display a very similar shape as those simulated with VD_{evap} and estimated from the measured points. In the low O:C case, we now see a slight underestimation of evaporation rate using the fresh VD_{PMF} and overestimation of evaporation rate with the RTC VD_{PMF}. A simple goodness of fit parameter like the mean squared error would not reflect the direction of this discrepancy as a qualitative description can. Looking at the revised Fig. 4a where we show only one brown line we feel that "matches well" describes well what we want to say.

11. Table 1 – The analysis appears to have used an accommodation coefficient of 1 to interpret the evaporation data (alpha in Table 1 versus the alpha in equation (3)). This was not discussed or justified (none of the values were in Table 1 were justified). There are papers that report smaller values for this system (e.g. Saleh et al. Env. Sci.

Tech.2013). How would reducing this value alter the results from the analysis? This should be discussed in the paper.

Answer: The theoretical framework used by Saleh et al., (2013) assumes that the mass-accommodation coefficient includes any mass transfer limitations caused by high viscosity of the particle phase. In Saleh et al., (2013) SOA growth and evaporation experiments were performed with α-pinene ozonolysis SOA at 10% RH. Based on the work of Li et al., (2019) it is likely that there are significant mass transfer limitations associated with this type of SOA and RH. Those mass transfer limitations likely decrease the mass-accommodation coefficient in Saleh et al., (2013).

In our work, we model the mass transfer limitations explicitly with the KM-GAP model and thus the mass-accommodation coefficient in our work consists of effects due to e.g. surface sticking which we neglect. Additionally, the work of Julin et al., (2014) reports near-unity mass-accommodation coefficients for various organic molecules based on molecular dynamic simulations and experiments.

We have added justification for the properties of the organic compounds presented in Table 1 as a footnote to the table

[b)] values are chosen to represent a generic organic compound with values similar to other α-pinene SOA studies (e.g. Pathak et al., 2007; Vaden et al., 2011; Yli-Juuti et al., 2017).

12. Figure 2 indicates little agreement in the “raw” volatility distributions between the PMF and evaporation approach. This is mentioned but not discussed in the text. The figure is also very confusing since there are overlaps in the volatility of the different PMFfactors (i.e. one you don’t show a volatility distribution of the PMF factors). I think it would be much clear if you lumped the factors together into a volatility distribution,using the colors to indicate the contribution of each factor to each bin (i.e. the volatility distribution would have stacked colored bars). Compared to Figure 2, there is better agreement in Figure 3 when the offers have lumped in the material into larger bins wider than one order of magnitude. That seems encouraging, but this lumping process and its justification was not\discussed in the text.

Answer: In Figure 2 we show the information from PMF analysis that we utilized in the model simulations. Therefore, the range of C* values for each factor is an important piece of information and we find that combining the factors in stacked bars would not convey this information as directly. Our motivation for the lumping process was that when we examine the “raw” volatility distribution of Figure 2, it is not evident if the two VD are similar as the reviewer also points out. One issue complicating the comparison is that the PMF analysis does not set uni-distant C^* values for the factors. The second point is that the FIGAERO samples can differentiate compounds with C^* values below -2. These compounds do not evaporate under the investigated isothermal evaporation conditions and are thus already grouped into the lowest volatility bin in VD_{evap}. We lumped both volatility distributions to volatility classes to study the similarities between the distributions on a qualitative level. The justification for the choice of these volatility classes is given in lines 325-328 of the manuscript. Finally, as a quantitative comparison we study what kind of evapograms the "raw" (i.e. "non-lumped") VD would produce. We have clarified our reasoning in the beginning of the results section on line 280-283:

We investigate the VD both on a qualitative and quantitative level. On a qualitative level we compare the amount of matter of different C^* *intervals. On a quantitative level we study what is the evaporation behavior of the particles based on the determined VD and how they compare to the measured evaporation.*

13. How different are the evapograms (Figure 4) when you use these different representations? A key issue is what level of information is there in the data. As I have discussed in earlier comment this problem seems very under constrained given the amount of data they have collected.

Answer: We do not use the three lumped volatility classes VD in the model simulations. The evapograms are always calculated with the "raw" VD (the one shown in Fig. 2). We hope that the modifications of the text mentioned above in comment 12 clarifies this.

14. Line 109 – What compounds were used to calibrate Tmax? The paper should provide a calibration curve showing these results.

Answer: We used polyethylene glycols (PEG) solutions in acetonitrile with 5 to 8 glycol units. As requested, we added the calibration curve and a brief description to the SI material.

15. Figure 4 – It is interesting that the PMF approach performs better for the mediumO:C aerosol compared to the low O:C aerosol. The PMF approach overestimates the evaporation of the This is mentioned on line 327, but only briefly discussed (~line500). The authors speculate it may be due to viscosity or particle phase chemistry. It Would be good to think about whether this indicates a shortcoming of the approach. For example, could this be due to the CIMS not detected a larger fraction of the less oxygenated aerosol? (This is related to some earlier comments).

Answer: The Figure 4 has changed in the revised version of the manuscript as we corrected the error in the T_{max}-C^* calibration. With the new parametrization it looks like the PMF approach (VD_{PMF}) performs better for the low O:C aerosol compared to medium O:C aerosol. In both oxidation conditions the evapogram calculated with VD_{PMF} of the fresh samples shows less evaporation than the measurements or the evapograms calculated with VD_{evap}.

The point raised by the reviewer is a valid one. The PMF method lumps all the organic compounds detected by the CIMS into preset number of factors. These factors are then treated as surrogate compounds when the evapograms are calculated with the LLEVAP model in Fig. 4. Given that in VD_{PMF} only one value is assigned to C^* of every PMF factor, it is not surprising that the VD_{PMF} does not produce an evapogram similar to the measurements.

Because the VD_{PMF} underestimates the evaporation, it seems possible that the iodide CIMS does not detect some fraction of the less oxygenated organic compounds, as we mentioned in our answer to comment 6. In our work, we expect that majority of the compounds are detected in the CIMS and the disagreement between measured and simulated evapograms in Fig. 4 comes from lumping the organic compounds into surrogate compounds in the PMF analysis or from the uncertainty in the conversion of desorption temperature to C*.

16. Figure 8. Optimized results (around line 440). The agreement seems impressive,but I suspect this is a just the result of fitting a model with lots of free parameters toa small set of data. Therefore, I am not surprised that the fit is great. If the fit is under constrained is this telling us anything about the technique? It was not clear if the authors had tested the applicability of the extracted values from this optimization against data the model had not been fit to? If this optimization is to be presented these issues must be discussed and some sort of cross-validation presented.

Answer: We agree that in the case of optimizing simultaneously C* and viscosity parameters there are a lot of free parameters (although neither C* or b_i are completely free parameters as they are restricted with minimum and maximum values) and therefore the estimates of parameter values from such optimizations should be interpreted with caution. However, our motivation with the low RH case was not to derive a universal parameterization. Our interest with the low RH data was to perform a cross-validation using a parametrization developed previously based on measurements of glass transition temperature of various organic compounds (DeRieux et al., 2018). Such validations of parameterizations against SOA dynamics are of importance if the parameterizations are to be used in the future e.g. for interpreting ambient or laboratory measurements or in large-scale model simulations of SOA formation. Our results show that the viscosity of SOA can be captured with this parametrization given the uncertainty in the parametrization and the C* values that we estimated using the same approach as with the high RH data. We have clarified our intent with the low RH experiments by adding following to lines 426-430

Our aim is to test if the slower evaporation, presumably due to higher viscosity of the SOA can be captured with a recently developed viscosity parametrization based on glass transition temperatures of various organic compounds (DeRieux et al., 2018). We also compare the results using the viscosity parametrization to an approach where we fit both the viscosity and VD to the evapogram.

17. Figure 8 –I interpret the dashed lines as the range of predications for the FIGAERO based approach (i.e., using the “theory” to predict viscosity). Is that correct? It is hard to tell what comparisons are based on truly independent comparison just using the FIGAERO versus fits of the data.

Answer: The reviewer is correct. We have added following clarification to the caption of Fig. 8

Grey lines show the minimum and maximum possible evaporation calculated with $VD_{PMF,dry}$ *(*C^* *of PMF factors calculated from* T_{max}*) and the highest (the original parametrization of DeRieux et al., (2018), grey dashed lines) or the lowest (30 K subtracted from the* T_g *of every ion, grey solid line) studied viscosity.*

18. Figure 8. Can’t differentiate between grey and black dashed lines.

Answer: We have changed the color of both lines to grey and changed one line to be solid and the other dashed.

References

Buchholz, A., Ylisirniö, A., Huang, W., Mohr, C., Canagaratna, M., Worsnop, D. R., Schobesberger, S. and Virtanen, A.: Deconvolution of FIGAERO-CIMS thermal desorption profiles using positive matrix factorisation to identify chemical and physical processes during particle evaporation, Atmos. Chem. Phys. Discuss., doi:https://doi.org/10.5194/acp-2019-926, 2019a.

Buchholz, A., Lambe, A. T., Ylisirniö, A., Li, Z., Tikkanen, O.-P., Faiola, C., Kari, E., Hao, L., Luoma, O., Huang, W., Mohr, C., Worsnop, D. R., Nizkorodov, S. A., Yli-Juuti, T., Schobesberger, S. and Virtanen, A.: Insights into the O:C-dependent mechanisms controlling the evaporation of α-pinene secondary organic aerosol particles, Atmos. Chem. Phys., 19(6), 4061–4073, doi:10.5194/acp-19-4061-2019, 2019b.

DeRieux, W.-S. W., Li, Y., Lin, P., Laskin, J., Laskin, A., Bertram, A. K., Nizkorodov, S. A. and Shiraiwa, M.: Predicting the glass transition temperature and viscosity of secondary organic material using molecular composition, Atmos. Chem. Phys., 18(9), 6331–6351, doi:https://doi.org/10.5194/acp-18-6331-2018, 2018.

Isaacman-VanWertz, G., Massoli, P., E. O’Brien, R., B. Nowak, J., R. Canagaratna, M., T. Jayne, J., R. Worsnop, D., Su, L., A. Knopf, D., K. Misztal, P., Arata, C., H. Goldstein, A. and H. Kroll, J.: Using advanced mass spectrometry techniques to fully characterize atmospheric organic carbon:

current capabilities and remaining gaps, Faraday Discussions, 200(0), 579–598, doi:10.1039/C7FD00021A, 2017.

Isaacman-VanWertz, G., Massoli, P., O’Brien, R., Lim, C., Franklin, J. P., Moss, J. A., Hunter, J. F., Nowak, J. B., Canagaratna, M. R., Misztal, P. K., Arata, C., Roscioli, J. R., Herndon, S. T., Onasch, T. B., Lambe, A. T., Jayne, J. T., Su, L., Knopf, D. A., Goldstein, A. H., Worsnop, D. R. and Kroll, J. H.: Chemical evolution of atmospheric organic carbon over multiple generations of oxidation, Nature Chem, 10(4), 462–468, doi:10.1038/s41557-018-0002-2, 2018.

Iyer, S., Lopez-Hilfiker, F., Lee, B. H., Thornton, J. A. and Kurtén, T.: Modeling the Detection of Organic and Inorganic Compounds Using Iodide-Based Chemical Ionization, J. Phys. Chem. A, 120(4), 576–587, doi:10.1021/acs.jpca.5b09837, 2016.

Julin, J., Winkler, P. M., Donahue, N. M., Wagner, P. E. and Riipinen, I.: Near-Unity Mass Accommodation Coefficient of Organic Molecules of Varying Structure, Environ. Sci. Technol., 48(20), 12083–12089, doi:10.1021/es501816h, 2014.

Lee, B. H., Lopez-Hilfiker, F. D., Mohr, C., Kurtén, T., Worsnop, D. R. and Thornton, J. A.: An Iodide-Adduct High-Resolution Time-of-Flight Chemical-Ionization Mass Spectrometer: Application to Atmospheric Inorganic and Organic Compounds, Environ. Sci. Technol., 48(11), 6309–6317, doi:10.1021/es500362a, 2014.

Li, Z., Tikkanen, O.-P., Buchholz, A., Hao, L., Kari, E., Yli-Juuti, T. and Virtanen, A.: Effect of Decreased Temperature on the Evaporation of α-Pinene Secondary Organic Aerosol Particles, ACS Earth Space Chem., 3(12), 2775–2785, doi:10.1021/acsearthspacechem.9b00240, 2019.

Lopez-Hilfiker, F. D., Mohr, C., D’Ambro, E. L., Lutz, A., Riedel, T. P., Gaston, C. J., Iyer, S., Zhang, Z., Gold, A., Surratt, J. D., Lee, B. H., Kurten, T., Hu, W. W., Jimenez, J., Hallquist, M. and Thornton, J. A.: Molecular Composition and Volatility of Organic Aerosol in the Southeastern U.S.: Implications for IEPOX Derived SOA, Environ. Sci. Technol., 50(5), 2200–2209, doi:10.1021/acs.est.5b04769, 2016.

Mohr, C., Lopez-Hilfiker, F. D., Yli-Juuti, T., Heitto, A., Lutz, A., Hallquist, M., D’Ambro, E. L., Rissanen, M. P., Hao, L., Schobesberger, S., Kulmala, M., Mauldin III, R. L., Makkonen, U., Sipilä, M., Petäjä, T. and Thornton, J. A.: Ambient observations of dimers from terpene oxidation in the gas phase: Implications for new particle formation and growth, Geophysical Research Letters, 2958–2966, doi:10.1002/2017GL072718@10.1002/(ISSN)1944-8007.GRLHIGHLIGHTS2017, 2018.

Pathak, R. K., Presto, A. A., Lane, T. E., Stanier, C. O., Donahue, N. M. and Pandis, S. N.: Ozonolysis of α-pinene: parameterization of secondary organic aerosol mass fraction, Atmos. Chem. Phys., 7(14), 3811–3821, doi:10.5194/acp-7-3811-2007, 2007.

Saleh, R., Donahue, N. M. and Robinson, A. L.: Time Scales for Gas-Particle Partitioning Equilibration of Secondary Organic Aerosol Formed from Alpha-Pinene Ozonolysis, Environ. Sci. Technol., 47(11), 5588–5594, doi:10.1021/es400078d, 2013.

Schervish, M. and Donahue, N. M.: Peroxy radical chemistry and the volatility basis set, Atmos. Chem. Phys., 20(2), 1183–1199, doi:10.5194/acp-20-1183-2020, 2020.

Vaden, T. D., Imre, D., Beránek, J., Shrivastava, M. and Zelenyuk, A.: Evaporation kinetics and phase of laboratory and ambient secondary organic aerosol., Proc. Natl. Acad. Sci. U.S.A., 108(6), 2190–2195, doi:10.1073/pnas.1013391108, 2011.

Yli-Juuti, T., Pajunoja, A., Tikkanen, O.-P., Buchholz, A., Faiola, C., Väisänen, O., Hao, L., Kari, E., Peräkylä, O., Garmash, O., Shiraiwa, M., Ehn, M., Lehtinen, K. and Virtanen, A.: Factors controlling the evaporation of secondary organic aerosol from α-pinene ozonolysis, Geophys. Res. Lett., 44(5), 2016GL072364, doi:10.1002/2016GL072364, 2017.

Comparing SOA volatility distributions derived from isothermal SOA particle evaporation data and FIGAERO-CIMS measurements

Olli-Pekka Tikkanen[1,2,3], Angela Buchholz[1], Arttu Ylisirniö[1], Siegfried Schobesberger[1], Annele Virtanen[1] and Taina Yli-Juuti[1]

[1]Department of Applied Physics, University of Eastern Finland, Kuopio, 70210, Finland
[2]Department of Agricultural Sciences, University of Helsinki, Helsinki, 00790, Finland
[3]Institute for Atmospheric and Earth System Research/Forest Sciences, Faculty of Agriculture and Forestry, University of Helsinki, Finland

Correspondence to: Olli-Pekka Tikkanen (olli-pekka.tikkanen@helsinki.fi)~~(op.tikkanen@uef.fi)~~

Abstract.

The volatility distribution of the organic compounds present in SOA at different conditions is a key quantity that has to be captured in order to describe SOA dynamics accurately. The development of the filter inlet for gases and aerosols (FIGAERO) and its coupling to chemical ionization mass spectrometer (CIMS) has enabled near simultaneous sampling of gas and particle phases of secondary organic aerosol (SOA) through thermal desorption of the particles. The thermal desorption data has recently been shown to be interpretable as a volatility distribution with the use of positive matrix factorization (PMF) method. Similarly, volatility distribution can be inferred from isothermal particle evaporation experiments, when the particle size change measurements are analyzed with process modelling techniques. In this study we compare the volatility distributions that are retrieved from FIGAERO-CIMS and particle size change measurements during isothermal particle evaporation with process modelling techniques. We compare the volatility distributions at two different relative humidity (RH) and two oxidation condition. At high RH conditions, where particles are in a liquid state, we show that the volatility distributions derived the two ways are similar~~comparable~~ within reasonable assumption of uncertainty in the effective saturation mass concentrations that are derived from FIGAERO-CIMS data. At dry conditions we demonstrate the volatility distributions are comparable in one oxidation condition and in the other oxidation condition the volatility distribution derived from the PMF analysis shows considerably more high volatility matter than the volatility distribution inferred from particle size change measurements. We also show that the Vogel-Tammann-Fulcher equation together with a recent glass transition temperature parametrization for organic compounds and PMF derived volatility distribution estimate are consistent with the observed isothermal evaporation under dry conditions within the reported uncertainties. We conclude that the FIGAERO-CIMS measurements analyzed with the PMF method are a promising method for inferring the organic compounds' volatility distribution, but care has to be taken when the PMF factors are interpreted. Future process modelling studies about SOA dynamics and properties could benefit from simultaneous FIGAERO-CIMS measurements.

1 Introduction

Aerosol particles have varying effects on health, visibility and climate (Stocker et al., 2013). Organic compounds comprise a substantial amount of atmospheric particulate matter (Jimenez et al., 2009; Zhang et al., 2007) of which a major fraction is of secondary origin, i.e., low-volatility organic compounds formed from oxidation reactions between volatile organic compounds (VOCs) and ozone, hydroxyl radicals and nitrate radicals (Hallquist et al., 2009). The aerosol particles containing these kind of oxidation products are called secondary organic aerosols (SOA) as opposed to primary organic aerosols i.e. organic particles emitted directly to the atmosphere. VOC oxidation reactions result in thousands of different organic compounds (Goldstein and Galbally, 2007)~~.~~ A recent review by Glasius and Goldstein, (2016) pointed out that our understanding of SOA is still lacking especially on formation and deposition, and their response to different physicochemical properties of the organic compounds such as volatility. In addition, also the phase state of the organic compounds has been shown to play a role in the SOA dynamics (Reid et al., 2018; Shiraiwa et al., 2017; Yli-Juuti et al., 2017; Renbaum-Wolff et al., 2013; Virtanen et al., 2010)

The physicochemical properties of organic aerosols can be studied directly and indirectly. The Aerodyne Aerosol mass spectrometer (AMS, Canagaratna et al., 2007; DeCarlo et al., 2006; Jayne et al., 2000) enabled direct and online composition measurements of atmospheric particles for the first time. Combining AMS data with statistical dimension reduction techniques such as factor analysis and positive matrix factorization (PMF; Zhang et al., 2011, 2007, 2005; Paatero and Tapper, 1994) allowed researchers to draw conclusions on sources and types of atmospheric organic particulate matter from the relatively complex mass spectra data.

The chemical ionization mass spectrometer (CIMS; Lee et al., 2014) coupled with the Filter Inlet for Gases and AEROsols (FIGAERO-CIMS, Lopez-Hilfiker et al., 2014) is a prominent online measurement technique to study both the gas and particle phases of SOA. During particle phase measurements, a key advantage over the AMS is the softer chemical ionization that retains much more of the molecular information of the compound than the electron impact ionization used in the AMS. Typically, the collection of the particulate mass is conducted at room temperature which minimiz~~s~~es the loss of semi-volatile compounds during collection. In addition to the overall chemical composition, the gradual desorption of the particulate mass from the FIGAERO filter yields the thermal desorption behavio~~u~~r of each detected ion, i.e., it is a direct measure of each ion's volatility. FIGAERO-CIMS measurements have been carried out in both laboratory and field environments to study SOA composition from different VOC precursors and in both rural and polluted environments (Breton et al., 2018; Huang et al., 2018; Lee et al., 2018; D'Ambro et al., 2017; Lopez-Hilfiker et al., 2015). However, the volatility information in these data sets have barely been used.

Besides direct mass spectrometer measurements, SOA properties have been inferred indirectly from growth (e.g. Pathak et al., 2007 and references therein) and isothermal evaporation (Buchholz et al., 2019a; D'Ambro et al., 2018; Yli-Juuti et al., 2017; Wilson et al., 2015; Vaden et al., 2011) measurements. The complexity of ~~the~~ organic compounds in these studies can be alleviated with the use of a volatility basis set (Donahue et al., 2006), where organic compounds are grouped based on their (effective) saturation concentration. However, the experimental setup also defines the range of C^* values that can be estimated from the data. ~~for example,,as~~ Vaden et al., (2011) and Yli-Juuti et al., (2017) have both shown that the volatility basis sets derived from SOA growth experiments result~~s~~ in too fast SOA evaporation compared to measured evaporation rates when the volatility basis set is used as input for~~in~~ process models. Possible reasons for such discrepancies include the different C^* ranges to which the SOA growth and SOA evaporation experiments are sensitive and the role of vapor wall losses in SOA growth experiments. This raises a need for alternative methods to derive organic aerosol volatility against which the volatilities inferred from the direct particle size measurements can be compared to.

Recently, Buchholz et. al., (2019b) demonstrated that the FIGAERO-CIMS measurements during particle evaporation can be mapped to a volatility distribution of organic compounds by conduction a PMF analysis. On the other hand, Tikkanen et al., (2019) showed that the volatility distribution can be inferred from isothermal particle evaporation measurements by optimizing evaporation model input to match the measured evaporation rate at different humidity conditions. In this study, we compare these two approaches for varying oxidation and particle water content conditions. Our main research questions are 1) Are the volatility distributions derived from particle size change during isothermal evaporation and from the FIGAERO-CIMS measurements similar~~comparable~~? 2) How to interpret the PMF results of FIGAERO-CIMS data in terms of volatility? 3) Can a recently published glass transition temperature parametrization (DeRieux et al., 2018) combined with the PMF analysis be used to model particle phase mass transfer limitation observed in evaporation at dry conditions, i.e., in the absence of particle phase water?

2 Methods

2.1 Experimental particle evaporation data

The experimental data we use is the same as reported in Buchholz et al., (2019a,b). We briefly summarize the measurement setup below. We generated the particles with a Potential Aerosol Mass (PAM) reactor (Kang et al., 2007; Lambe et al., 2011) from the reaction of α-pinene with O_3 and OH at three different oxidation levels (average oxygen-to-carbon O:C ratios of 0.53, 0.69, and 0.96). We focus on the lowest O:C (0.53) and medium O:C (0.69) experiments in this work. The closer analysis of the high O:C experiments suggest particle phase reactions during the evaporation (Buchholz et al., 2019a,b). To avoid the uncertainty that would arise from unknown particle phase reactions, we chose not to include the high O:C data in our analysis.

We chose a monodisperse particle population (mobility diameter d_p = 80 nm) with two nano tandem type differential mobility analyzers (nano-DMA; TSI inc., Model 3085) from the initial polydisperse particle population. The size selection diluted the gas phase initiating particle evaporation. The monodisperse aerosol was left to evaporate in a 100 L stainless steel residence time chamber (RTC). We measured the particle size distribution during the evaporation with a scanning mobility particle sizer (SMPS; TSI inc., Model 3082+3775). The RTC filling took approximately 20 minutes and we performed the first size distribution measurement in~~at~~ the middle of the filling interval. To obtain short residence time data (data before 10 minutes of evaporation) we added a bypass to the RTC which led the sample directly to the SMPS. By changing the length of the bypass tubing, we were able to measure the particle size distribution between 2 s and 160 s of evaporation. We measured the isothermal evaporation up to 4 – 10 hours depending on the measurement. We performed the measurements for each oxidation level both at high relative humidity (RH = 80%) and at dry conditions (RH < 2 %). The change in particle size with respect to time are called evapograms. In an evapogram, the horizontal axis presents evaporation time and vertical axis shows the evaporation factor (EF), i.e., measured particle diameter divided by the initially selected particle diameter.

To classify the oxidation level of the particles, we derived the average O:C ratio from composition measurements with a High-Resolution Time-Of-Flight Aerosol Mass Spectrometer (AMS, Aerodyne Research Inc.). Further, we conducted detailed particle composition measurements with an Aerodyne Research Inc. FIGAERO, (Lopez-Hilfiker et al., 2014) coupled with a chemical ionization mass spectrometer (CIMS) with iodide as the reagent ion (Aerodyne Research Inc., Lee et al., 2014). Previous studies using FIGAERO-CIMS with iodide as the reagent ion found 50% or better mass closure compared to more established methods of quantifying OA mass (albeit with high uncertainties; **Isaacman-VanWertz et al., (2017); Lopez-Hilfiker et al., (2016))**. Therefore, it appears that the bulk of reaction products expected from a-pinene oxidation contains the functional groups required for detection by our FIGAERO-CIMS.

In the FIGAERO inlet, particles are first collected on a PTFE filter. Then the collected particulate mass desorbs slowly due to gradually heated nitrogen flow which is then transported into the CIMS for detection. We derived the average chemical composition of the particles by integrating the detected signal of each ion over the whole desorption interval. For each ion, the change of detected signal with desorption temperature is called thermogram and generally, the temperature at the maximum of the thermogram (T_{max}) is correlated to the volatility of the detected ion. Similar to Bannan et al., (2019) and Stark et al., (2017), we calibrated the T_{max} - volatility relationship using compounds with known vapour pressure. The calibration procedure is described in the supplementary material.

We collected particles for FIGAERO-CIMS analysis at two different stages of the evaporation. We refer to these samples ~~stages~~ as either “fresh” or “RTC” samples. The fresh samples were collected for 30 minutes directly after the selection of the monodisperse population. The RTC samples were collected after 3 to 4 hours of evaporation in the RTC for 75 minutes. The collected particulate mass was 140–260 ng and 20–70 ng for fresh and RTC samples, respectively. More details about sample collection, desorption parameters, and data analysis can be found in Buchholz et al., (2019a).

2.2 The volatility distribution

We represent the myriad of organic compound in the SOA particles with a one-dimensional volatility basis set (1D VBS, below only VBS, Donahue et al., 2006). The VBS groups the organic compounds into ‘bins’ based on their effective (mass) saturation concentration C^*, defined as the product of the compounds activity coefficient and saturation concentration. Generally, a bin in the VBS represents the amount of organic material in the particle and gas phases. In our study, the walls of the RTC have been shown to work as an efficient sink for gaseous organic compounds (Yli-Juuti et al., 2017). Thus, we can assume that the gas phase in our experimental setup does not contain organic compounds, i.e., the amount of organic matter in a bin is the amount in the particle phase. To distinguish from a traditional VBS that groups the organic compounds to bins where there is a decadal difference in C^* between two adjacent bins, we call the VBS in our work a volatility distribution (VD). We present the amount of material in each VD bin as dry mole fractions, i.e., mole fractions of the organics, excluding water. In the analysis presented below, we assign properties to each VD bin (e.g. molar mass) treating each bin as if it consisted of only a single organic compound with a single set of properties. We label these pseudo-compounds as “VD compounds” to distinguish them from real organic compounds. The physicochemical properties of each VD compound are listed in Table 1 as well as the ambient conditions of each evaporation experiment.

2.3 Deriving volatility distribution from an evapogram

We followed the similar approach as in Yli-Juuti et al., (2017) and Tikkanen et al., (2019) to derive a VD at the start of the evaporation from an evapogram. To model the evaporation at high RH, we used a process model (liquid-like evaporation model, hereafter LLEVAP) that assumes a liquid-like particle, i.e., a particle where there are no mass transfer limitations inside the particle and where the rate of change of the mass of a VD compound in the particle phase can be calculated directly from the gas phase concentrations of this VD compound near the particle surface and far away from the particle (Vesala et al., 1997; Lehtinen and Kulmala, 2003; Yli-Juuti et al., 2017). In this case, the main properties defining the evaporation rate are the saturation concentrations of each VD compound and their amount in the particle.

We used the LLEVAP model to characterize the volatility ranges interpretable from the evaporation measurements. We calculated the limits by modelling evaporation of a hypothetical particle that consists of one organic compound at dry conditions iterating the range of $\log_{10}(C^*)$ values from -5 to 5. We determined the minimum C^* value with “detectable evaporation”, i.e., at least 1% change in particle diameter during the evaporation time (up to 6 h) and the maximum C^* value before “complete evaporation” occurred, i.e., 99% evaporation within 10 s. The minimum $\log_{10}(C^*)$ calculated with this method was -3 ~~µgm^{-3}~~ and the maximum– $\log_{10}(C^*)$ was 2. We then modelled the particle composition with six VD compounds with C^* values between these minimum and maximum values. Each VD compounds has a decadal difference in

C^* to adjacent VD compounds (the traditional VBS). We note that based on this analysis all the compounds with $\log_{10}(C^*) < -3$ will not evaporate during the experimental time scale. This means that any compounds with lower C^* than this threshold will be assigned to the $\log_{10}(C^*) = -3$ VD compound. Similarly, any compound with $\log_{10}(C^*) > 2$ will be classified into the $\log_{10}(C^*) = 2$ VD compound or not be detected at all due to evaporating almost entirely before the first measurement point.

We calculated the dry particle mole fraction of each VD compound at the start of the evaporation by fitting the evaporation predicted with the process model to the measured evapograms. Our goal was to minimize the mean squared error in vertical direction between the experimental data and the LLEVAP output. We used the Monte Carlo Genetic Algorithm (MCGA, Berkemeier et al., 2017; Tikkanen et al., 2019) for the input optimization. In the optimization, we set the population size to be 400 candidates, number of elite members to 20 (5% of the population), number of generations to 10, and number of candidates drawn in the Monte Carlo (MC) part to 3420 which corresponds to half of the total process model evaluations done during the optimization. We performed the optimization 50 times for each evapogram and selected the best fit VD estimate for further analysis.

The VD derived from the evapograms are hereafter referred to as the VD_{evap}. The initial composition of the SOA particles in the dry and wet experiments were the same and can be described by the same fitted VD_{evap} as the particles were generated at the same conditions in the PAM and only the evaporation conditions changed.

2.4 Deriving volatility distribution from FIGAERO-CIMS measurement

As shown by Bannan et al., (2019) and Stark et al., (2017), the peak desorption temperature, T_{max}, can be used together with careful calibration to link desorption temperatures from the FIGAERO filter to C^* values for the detected ions. In principle, this would allow us to assign one C^* value to each ion thermogram. But this assumes that one detected ion characterized by its exact mass is indeed just one compound. In practice, this is not always the case and for some ion thermograms a bimodal structure or distinct shoulders/broadening are visible. This can be caused by isomers of different volatility which cannot be separated even by high resolution mass spectra.

Another complication arises due to the thermal desorption process delivering the collected aerosol mass into the CIMS. Especially multi-functional, and hence low volatility compounds may thermally decompose before they desorb from the filter, and thus be detected as smaller ions. The apparent desorption temperature is then determined by the thermal stability of the compound and not its volatility. Typically, this decomposition processes start at a minimum temperature and will not create a well-defined peak shape (Buchholz et al., 2019b, Schobesberger et al., 2018) presumably because an observed decomposition product may have multiple sources, especially when including all isomers, and the ion signal for the respective composition may overlap with the signal of isomers derived from true desorption. E.g., a true constituent of the SOA particle may give rise to an observed main thermogram peak, but it may be broadening and/or tailing if a decomposition product has the same composition. By ignoring this and simply using the T_{max} values, the true volatility of the SOA particle constituents will be overestimated, i.e., the derived VD will be biased towards higher C^* bins.

One more potential source of bias is our implicit assumption of a constant sensitivity of the CIMS towards all compounds, which follows from the lack of calibration measurements for our datasets (which indeed is a challenging endeavour; e.g., **Isaacman-VanWertz et al., (2018))**. It is plausible that less volatile compounds tend to be detected at higher sensitivity **(Iyer et al., 2016; Lee et al., 2014)**, up to a kinetic limit sensitivity. Consequently, a volatility distribution derived from FIGAERO-CIMS thermograms may be biased towards lower volatility (C^* bins), at least for compositions not associated with thermal decomposition.

To separate the multiple sources possibly contributing to each ion thermogram (isomers and thermal decomposition products), we applied the Positive Matrix Factorisation (PMF, Paatero and Tapper, 1994) to the FIGAERO-CIMS data set. PMF is a well-established mathematical technique in atmospheric science mostly used to identify the contribution of different sources of aerosol particle constituents~~s~~ or trace gases in the atmosphere. PMF represents the measured matrix of time-series of mass spectra, $\boldsymbol{X}$, as a linear combination of a (unknown) number of constant source profiles, $\boldsymbol{F}$, with varying contributions over time, $\boldsymbol{G}$:

$$\boldsymbol{X} = \boldsymbol{G} \cdot \boldsymbol{F} + \boldsymbol{E} \qquad (1)$$

$\boldsymbol{E}$ is a matrix containing the residuals between the measured ($\boldsymbol{X}$) and the fitted data ($\boldsymbol{G \cdot F}$). Values for $\boldsymbol{G}$ and $\boldsymbol{F}$ are found by minimising this residual, $\boldsymbol{E_{ij}}$, scaled by the corresponding measurement error, $\boldsymbol{S_{ij}}$, for each ion i at each time j

$$Q = \sum_{i=1}^{m} \sum_{j=1}^{n} \left(\frac{E_{i,j}}{S_{i,j}} \right) \qquad (2)$$

Each row in $\boldsymbol{F}$ contains a factor mass spectrum and each column in $\boldsymbol{G}$ holds the corresponding time series of contribution by each factor. In the case of FIGAERO-CIMS data, the time series is equivalent to the desorption temperature ramp during the thermogram~~,~~ and will be called “mass loading profile” below. The absolute values (temperature or time) are irrelevant for the performance of PMF as the “x values” are only used to determine the order of the data points but have no influence on the model output (Paatero and Tapper, 1994). This allowed us to combine multiple separate thermogram measurements into one data set and conducting a PMF analysis. This simplified the comparison of factors between measurements. More details about the PMF method in the specific case of FIGAERO-CIMS data can be found in Buchholz et al., (2019b).

Once the PMF algorithm was applied to the FIGAERO-CIMS data we calculated the VD from the mass loading matrix $\boldsymbol{G}$. We interpolated each factor’s mass loading profile with a resolution of 100 sample points between two temperature steps to gain sufficient statistics for further analysis. T_{max} was determined as the temperature of the maximum of the factor mass loading series. We integrated the factor mass loading profile and defined the temperatures where the value of the integral reaches 25% and 75% of its maximum value. This temperature interval formed the factors desorption temperature range and the corresponding C^* values will be used in Sect. 3.3. We converted the T_{max} values into ~~a~~ C^* values and the desorption temperature range into a C^* range with ~~the~~a parametrization ~~based~~ derived from calibration measurements (see Supplementray material for details) with organic compounds with known C^* values.

$$C^* = \frac{\exp\left(\alpha + \beta T_{factor}\right) M_{org}}{R\, T_{ambient}} 10^9 \qquad (3)$$

where C^* is the effective saturation concentration in units $\mu g m^{-3}$, M_{org} is the molar mass of the organic compound assumed to be M_{org} = 0.2 kg mol^{-1}, R is the universal gas constant, T_{factor} (in °C in Eq. 3) is the temperature of the~~in~~ mass loading profile and $T_{amibent}$ (in Kelvin in Eq. 3) is the ambient temperature where the evaporation happens (see Table 1), α and β are the fitted coefficients from the calibration data α=(-1.431±0.31~~0.618±3.739~~) and β=(~~9±0.0035-0.1~~-0.207±0.006) °C~~K~~$^{-1}$. We applied the lower and higher bounds of the fitting coefficients' uncertainty when we calculated the ~~minimum and maximum for the allowed~~ C^* range in~~values in~~ Sect 3.3. Finally, the signal fraction of each factor was calculated by dividing the integral of a factor's signal over the whole temperature range with the sum of integrals of ~~all factors' signals~~all factors. We compare this signal fraction to the dry mole fraction in the VD_{evap}. We refrained from converting the counts per second signal into moles as no adequate transmission and sensitivity measurements were available for the used FIGAERO-CIMS setup. We refer the volatility distribution calculated from the PMF data using the T_{max} values of each factor as VD_{PMF} later in this work.

With Eq. (3)~~T_{max} calibration the~~, we can calculate the minimum and maximum C^* values that can be resolved from a FIGAERO thermogram. The desorption temperature was ramped between 27 °C and 200 °C, but defined peaks (and thus T_{max} values can be detected only between 30 and 180 °C. Thus, the resolvable $\log_{10}(C^*)$ values range from 1.6 to -11.9~~1.7 to -11.1~~. It has to be kept in mind that strictly this calibration only applies to the T_{max} values of a single ion thermogram.

2.5 Modelling particle viscosity at dry conditions

To model the mass transfer limitations observed in the evaporation measurements at dry conditions (Buchholz et al., 2019a) we used the Kinetic multilayer model for gas particle interactions (KM-GAP; Shiraiwa et al., 2012) with modifications described in Yli-Juuti et al., (2017) and Tikkanen et al., (2019). The main modification~~s~~ to the original model was that during evaporation the topmost layer (the quasi static surface layer) merges with the first bulk layer if the thickness of the layer is smaller than 0.3 nm. We calculated the viscosity at each layer of the particle as

$$\log_{10}(\eta_j) = \sum_{i=1}^{N} X_{mole,i,j} \log_{10}(b_i), \qquad (4)$$

where $X_{mole,i,j}$ is the mole fraction of the VD compound i in layer j and b_i is a coefficient that describes the contribution of each VD compound to the overall viscosity.

Since we generated the particles in the same environment (PAM chamber) and only the evaporation happened~~ed th~~ at different conditions, the VD at the start of the evaporation derived from high RH data represents also the composition at the start of the evaporation at dry conditions. Then we can use the best fit VD_{evap} from the high RH data as input for KM-GAP and fit the b_i values in Eq. (4) to the dry data set. We set the minimum and maximum allowed values for b_i to 10^{-15} and 10^{20}, respectively. To estimate the b_i values when modelling the evaporation with VD_{PMF} at dry conditions, we calculated these b_i terms using the mass spectra of each factor ($\boldsymbol{F}$ in Eq. 1) and the Vogel-Tammann-Fulcher (VTF) equation (DeRieux et al., 2018; Angell, 2002, 1995)

$$\eta_i=\eta_\infty \exp\left(\frac{T_{0,i}D}{T-T_{0,i}}\right), \tag{5}$$

where η_i is the viscosity of a VD compound / PMF factor i which can be seen as a proxy for b_i in an ideal solution, η_∞ is the viscosity at infinite temperature, $T_{0,i}$ is the Vogel temperature of i, and D is a fragility parameter. Setting $\eta_\infty = 10^{-5}$ Pa s and $\eta(T_g) = 10^{12}$ Pa s (e.g. DeRieux et al., 2018; Gedeon, 2018), where T_g is the glass transition temperature of a compound yields

$$T_{0,i}\approx\frac{39.14\,T_{g,i}}{39.14+D}. \tag{6}$$

We calculated T_g for every compound in the PMF mass spectra with a parametrization for SOA matter developed by DeRieux et al., (2018). We then computed T_g for each PMF factor as a mass fraction weighted sum of glass transition temperatures of individual compounds (DeRieux et al., 2018; Dette et al., 2014). Based on the $T_{g,i}$ for each PMF factor we calculated the viscosity of each PMF factor with Eqs. (5) and (6) and used them as an approximation for b_i. We used fragility parameter value D = 10 according to DeRieux et al., (2018).

3 Results

In this section we first focus on the high RH experiments where evaporation is modelled with the LLEVAP model. We will first compare VD_{evap} and VD_{PMF} when the C^* of a PMF factor is determined from the factor's T_{max}. Then, we compare the volatility distributions where the C^* of a PMF factor is determined as a~~the~~ range from the 25th and 75th percentile desorption temperatures. Lastly, we study~~compare~~ the volatility distributions at dry conditions. We investigate the VD both on a qualitative and quantitative level. On a qualitative level we compare the amount of matter of different C^* intervals relevant for the evaporation process. On a quantitative level we study what is the evaporation behavior of the particles based on the determined VD and how they compare to the measured evaporation.

3.1 PMF solution interpretation

Figure S2~~1~~ ~~and Fig S2~~ shows ~~all~~ mass loading profiles derived from FIGAERO-CIMS measurements ~~of evaporation~~ of medium and low O:C particles at high RH. The corresponding factor mass spectra can be found in Fig. S3~~3~~ and Fig. S4~~4~~. A key step in any PMF analysis is determining the "right" number of factors as this can affect the interpretation of the results. A 7-factor solution was chosen for the medium O:C cases and a 9-factor solution for the low O:C ones (see Buchholz 2019b for details). Two additional factors in the low O:C case were needed to capture a contamination on the FIGAERO filter during the dry, fresh sample (factors LC1 and LC2 in Fig. S2~~1~~ and Fig. S4~~2~~). As these two factors were clearly an artifact~~artefact~~ introduced by the FIGAERO filter sampling, we omitted their contribution ~~the data setfrom~~ for the following analysis. From careful comparison of the factor profiles and mass spectra with filter blank measurements, we determined that factor MB1 in medium O:C case and factor LB1 in low O:C case describe the filter/instrument background and are thus also excluded from the VD comparison presented below.

Factors 1-5 in both O:C cases ~~-~~exhibit a monomodal peak shape and can thus be characteriz~~s~~ed by their T_{max} values, factor MD1 in medium O:C case and factor LD1 in low O:C case needs to be investigated more closely, as its factor mass spectrum and the sometimes bimodal mass loading profile suggest that this factor contains compounds stemming from both direct desorption (desorption T<100 °C) and thermal decomposition (desorption T~~-~~>100 °C, see Buchholz et al., 2019b for details). To account for this, the factor is split into two with the first half containing the signal from desorption temperature below 100 °C (factor M/LD1a) and the second half containing that above 100 °C (factor M/LD1b). We treat these factors separately. We note that now the latter half of the split factor is dominated by thermal decomposition products so that the apparent desorption temperature is actually the temperature at which thermal decomposition leads to products which desorb at this temperature. This apparent desorption temperature is thus a lower limit for the decomposing parent compound, i.e., the true volatility of these parent compounds is even lower. However, the desorption temperatures are so high that they lead to $\log_{10}(C^{*}) < -3$ and are thus below the comparable range for VD_{evap}. Figure 1 (high RH data) and Fig. S10~~5~~ (dry condition data) show the mass loading profiles derived from FIGAERO-CIMS measurements of medium and low O:C particles~~,~~ ~~evaporation~~ after we excluded the contamination and background factors and split the decomposition factors.

3.2 Volatility distribution comparison at high RH based on factor T_{max}

To compare VD_{evap} and VD_{PMF}, we need to determine the time interval in the evapogram that the VD_{PMF} represents. We collected the fresh samples directly after the size selection. As the particles were collected on a filter for 30 minutes, the collected sample represents particles that have evaporated from 0 up to 30 minutes in the organic vapour free air. We note that this is different from the standard FIGAERO-CIMS sample collection where particles are collected in a quasi-equilibrium with the surrounding gas phase and no significant evaporation occurs (Lopez-Hilfiker et al., 2014). For RTC samples, we need to consider also that not all particles have evaporated for the same time due to the filling of the RTC for ca. 20 minutes. We determined the minimum time the particles have evaporated in the RTC as the time when we started the sample collection minus the RTC filling time. We determined the maximum evaporation time in the RTC to be the time when we stopped the sample collection plus the filling time. These minimum and maximum comparison times are shown in Table S1~~2~~ and they are referred to as minimum and maximum (sample) evaporation time. The mean (sample) evaporation time is defined to be~~In addition, we also compare the volatility distributions~~ at the middle of the sample collection interval~~, i.e., the mean (sample) evaporation time~~. For simplicity we will show in the main text the results from analysis where the FIGAERO-CIMS samples were assumed to represents the particles at the mean sample evaporation time. We show the analysis where the samples were assumed to represent the particles at minimum and maximum evaporation time in the supplementary material.

Figure 2 shows VD$_{\mathrm{evap}}$ and VD$_{\mathrm{PMF}}$ for medium (Fig. 2a-b) and low O:C (Fig. 2c-d) particles at high RH. In the VD$_{\mathrm{PMF}}$ calculated from T$_{\mathrm{max}}$~~,~~ value~~s~~ of each factor (black crosses), the factors fall into three different volatility classes within our chosen particle size and experimental time scale: practically non-volatile ($\log_{10}(C^*) \leq -2$~~)~~, slightly volatile ($-2 < \log_{10}(C^*) \leq 0$,) and volatile ($\log_{10}(C^*) > 0$). We use these three volatility classes to compare the volatility distributions in Fig. 3 where each VD compound are grouped to these three volatility classes. Figure 3 presents the VD$_{\mathrm{PMF}}$ where C* of each factor is calculated from the T$_{\mathrm{max}}$ value and compares this VD$_{\mathrm{PMF}}$ to what VD$_{\mathrm{evap}}$ is at the ~~minimum,~~ mean~~ and maximum~~ time the FIGAERO samples had evaporated. We show the same comparison for minimum and maximum evaporation time in Fig. S5 and Fig. S6.

After the volatility class grouping is applied, we see that there are differences between VD$_{\mathrm{evap}}$ and VD$_{\mathrm{PMF}}$. With VD$_{\mathrm{PMF}}$ of the fresh samples there are excess amount of matter in the lowest volatility class (volatility class 1) and less material in the volatility class 2 compared to VD$_{\mathrm{evap.}}$ In both oxidation condition. ~~there is an excess amount of matter in the highest volatility class (volatility class 3) of the VD$_{\mathrm{PMF}}$ compared to the VD$_{\mathrm{evap}}$-~~ In addition, the low O:C fresh sample shows more material in the volatility class 3 in VD$_{\mathrm{PMF}}$ compared to VD$_{\mathrm{evap}}$.~~in all the cases~~. ~~Fig. 3) the VD$_{\mathrm{PMF}}$ does not directly match any of the VD$_{\mathrm{evap}}$. For particles with medium O:C, VD$_{\mathrm{PMF}}$ shows more contribution of volatility class 2 and less of in volatility class 1 compared to VD$_{\mathrm{evap}}$. and Fig. 3), the VD$_{\mathrm{PMF}}$ seems to be the closest to the VD$_{\mathrm{evap}}$ at the very start of the evaporation. With the RTC samples (Fig. 3band With the fresh samples (Fig. 3~~

To investigate the observed discrepanci~~y~~es furthe~~r~~r~~more detailed~~, we used the VD$_{\mathrm{PMF}}$ shown in Fig 2 as an input to ~~for~~ the LLEVAP model and calculated the corresponding isothermal evaporation behavior (i.e. the evapogram). We show these simulated evapograms in Fig. 4a for the medium O:C case and in Fig 4b for low O:C condition together with the simulated evapogram calculated using VD$_{\mathrm{evap}}$ as an input for~~for~~ the LLEVAP model. ~~The derived VD$_{\mathrm{PMF}}$ represents the particle composition averaged over the sample collection interval. To account for this, we run the model by starting the evapogram~~

~~simulations calculated with VD$_{PMF}$ either at the start of this interval (minimum isothermal evaporation before sample collection), at the mean (mean isothermal evaporation before sample collection), or at the end (maximum isothermal evaporation before sample collection).~~ The simulated evapograms calculated with VD$_{PMF}$ of the fresh samples do not match the measured evapograms predicting less evaporation, while the evapogram calculated with VD$_{evap}$ agrees well with the experimental evapogram (black lines in Fig. 4), as ~~we~~ expected since this is~~was~~ the goal of the VD$_{evap}$ determination. The simulation calculated with VD$_{PMF}$ of the fresh sample (light blue lines in Fig. 4 for mean evaporation time and Fig. S7 for other evaporation times) shows slower evaporation than the observations or the simulation calculated with VD$_{evap}$.. This is consistent with the results show in Fig. 3 where the VD$_{PMF}$ contained more low volatility material than the VD$_{evap}$. ~~). If VD$_{PMF}$ is set to be the particle composition at mean or maximum evaporation time the simulated evaporation is faster than the measured one. 4 as the particle composition at minimum evaporation time, the simulated evaporation is slower than the measured evaporation (light blue lines in Fig. 'If we take the VD$_{PMF}$ of the fresh samples~~

Figure 4 shows also the simulated evapograms calculated with VD$_{PMF}$ of the RTC samples (light brown lines in Fig. 4 and Fig. S7). in these cases, the particles size decreases little within the simulation time scale. With medium O:C particles, the simulated evaporation matches well~~better~~ to the measured evaporation. ~~than the simulations calculated with the VD$_{PMF}$ of the fresh sample although the simulated evapograms shows a slightly higher rate of evaporation than what is measured.~~ With low O:C particles, the evaporation calculated with VD$_{PMF}$ is too fast. The shape of the evapogram does not match the measured one.

3.3 Applying desorption range to characterize the volatility of PMF factors

The T$_{max}$ value is a practical choice for the characteristic temperature of the desorption process. However, as we saw on Sect. 3.2~~1~~ the VD$_{PMF}$ calculated from the peak desorption temperatures did not produce the measured evapogram when used as an input to the LLEVAP model. Working under the assumption that all material collected on the FIGAERO filter, including the higher volatility material, is detected in the CIMS and then captured in the PMF analysis we will relax the assumption that the volatility of the factor is characterized strictly by the T$_{max}$ value of the factor and investigate the VD$_{PMF}$ further. We will explore how the VD$_{PMF}$ changes when the desorption temperature and the resulting C* are interpreted to contain uncertainty and if the VD$_{PMF}$ considering these uncertainty ranges is consistent with the observed isothermal evaporation. The uncertainty in the desorption temperature raises from the facts that compounds volatilize~~volatilise~~ from the FIGAERO filter throughout the heating and, therefore, one value might not be adequate to characterize the C* of a factor and that each PMF factor contains multiple compounds with distinct C*.

We calculated the 25th and 75th percentiles of the desorption temperatures of each factor and converted them to effective saturation concentrations as described in section 2.4 (see diamond markers in Fig. 1). We show the resulting C* ranges in Fig. 2 as horizontal solid lines where the line colour matches the ~~factor's~~ colour of the factors in Fig. 1. We then ran MCGA optimization by setting a number of compounds equal to the number of PMF factors, molar fraction for each compound at the FIGAERO-CIMS sampling time fixed to the molar fraction of the corresponding factor and set the C^* as the optimized variables restricted to the range corresponding to the 25th and 75th percentile desorption temperature. In the optimization the goodness-of-fit statistics was calculated as a mean squared error similar to the determination of VD_{evap}.

As the fresh samples were collected between 0 and 30 minutes from the start of the evaporation, we sought for a fitting set of C^* values for ~~for~~ evaporation starting at 0, 15~~,~~ and 30 minutes. We show the results for the mean sample evaporation time (15 min) in the main text and the other evaporation times in the supplementary material. Due to scarcity of particle size measurements at collection time of the RTC sample, we will apply this analysis only to the VD_{PMF} of the RTC sample at its minimum evaporation time. In each optimization we set the initial particle diameter to be the same as what is simulated with VD_{evap}. We derived 50 C^* estimates for both samples and each evaporation time. From these 50 estimates we chose the best fit evapogram. We refer to these optimized volatility distributions as $VD_{PMF,opt}$ to separate them from the VD_{PMF} where we used T_{max} to characterize C^* of a PMF factor.

We show the optimized C^* values forming $VD_{PMF,opt}$ in Table 2~~3~~ (see Table S2 for minimum and maximum sample evaporation times) ~~for all the studied cases~~. Figure 5~~a~~ shows the best fit evaporation simulations calculated with $VD_{PMF,opt}$ ~~of the medium O:C fresh sample~~. The other sample evaporation times are displayed in the supplementary material Fig. S8. ~~All the simulated evapograms~~ For both oxidation condition, the simulations were the fresh sample is set to represent the evaporating particles at mean or maximum sample evaporation time resemble the experimental evapogram and evapogram calculated with VD_{evap}, ~~.~~ although the simulation in medium O:C condition shows a 5 times larger goodness-of-fit compared to the simulation calculated with VD_{evap}. The simulations starting from maximum evaporation time of the fresh samples show similar results while the simulations starting from the minimum sample evaporation time results in too slow evaporation (Fig. S8). The evapograms determined with the $VD_{PMF,opt}$ of the RTC samples agree with the measured evaporation as well. ~~shows faster evaporation than the measurements.~~

~~from the point of 30 minutes of isothermal evaporation does not match the measured evapogram butmatch the experimental evapogram and the simulated evapogram using VD_{evap} as input. The evapogram using $VD_{PMF,opt}$ startings. The evapograms initialized at 0 min and15 min low O:C sampleforhe simulated evapograms calculated with $VD_{PMF,opt}$ Figure 5b shows t~~

~~For finding the $VD_{PMF,opt}$ for the low O:C RTC sample starting at minimum sample evaporation time (168 minutes) we needed to exclude factor LD1a from the calculations to be able to derive the $VD_{PMF,opt}$. As Buchholz et al., (2019b) reported, the mass spectrum of factor LD1a is dominated by compounds that come from the FIGAERO filter / instrument background. In low O:C RTC sample factor L1a is present at such high relative signal strength that its mole fraction is significant to other factors even though the absolute signal strength does not change drastically between the fresh and the RTC sample. The high relative contribution of factor LD1a is most probably due to the low amount of organic matter available for sample collection.~~

Overall, these results demonstrate that the information derived from the fresh and RTC FIGAERO-CIMS samples can describe the volatility ~~composition~~ of the evaporating particles, when uncertainty in the desorption temperature are considered.

3.4 Comparison of the volatility distribution of the fresh and RTC sample at high RH

In this section, we compare $VD_{PMF,opt}$ of the fresh samples to VD_{PMF} of the RTC sample to study if~~are~~ the two VD are ~~comparable~~similar. We compare the two VD at the mean evaporation time of the RTC sample. We calculated the evapograms with $VD_{PMF,opt}$ of the fresh sample as the initial particle composition ~~starting from different sample evaporation times~~ and recorded the mole fraction of each factor at mean evaporation time of the RTC sample (216 minutes for medium O:C particles and 211 minutes for low O:C particles). Figure 6a and Fig. 6c show this comparison for both medium O:C and low O:C particles.~~, where t~~ The factors are grouped into the three volatility classes described in Sect. 3.2. In Fig. 6 we show the results from the analysis where $VD_{PMF,opt}$ was optimized by assigning the fresh sample composition at the mean sample evaporation time. Similar comparison using minimum and maximum evaporation time of the fresh sample is given in Fig. S9. To ensure that the factors are grouped to the same volatility classes for each studied VD, we used the C^* values of the $VD_{PMF,opt}$ at mean sample evaporation time as basis according to which the grouping is done.

Assuming that the fresh sample represents particles from the middle of the sampling interval (mean evaporation time), the compositions simulated based on the $VD_{PMF,opt}$ of the fresh samples are comparable to the corresponding VD_{PMF} of the RTC sample in both oxidation conditions (Fig. 6). The agreement is good especially for the low O:C case for which the $VD_{PMF,opt}$ show a slightly smaller contribution in volatility class 1 and corresponding higher contribution in volatility class 2 compared to the VD_{PMF} of the RTC sample (Fig. 6c). For medium O:C case, the $VD_{PMF,opt}$ predicted higher contribution of volatility class 1 and lower contribution of volatility class 2 compared to VD_{PMF} (Fig 6a). For~~In~~ medium~~both~~ O:C conditions~~levels~~, the agreement between $VD_{PMF,opt}$ and VD_{PMF} improved when using the $VD_{PMF,opt}$ of maximum fresh sample evaporation time, while $VD_{PMF,opt}$ of minimum fresh sample evaporation time show higher contribution of volatility class 2 and lower contribution of volatility class 1 compared to ~~than~~ the VD_{PMF} of the RTC sample. ~~Contrary, the $VD_{PMF,opt}$ of maximum fresh sample evaporation time in the medium O:C case (Fig. 6a) shows higher contribution of volatility class 1 and lower contribution of volatility class 2 than the VD_{PMF} of the RTC sample. These results show that even though we calculated the $VD_{PMF,opt}$ starting from the minimum and maximum possible sample evaporation time, the $VD_{PMF,opt}$ of the fresh samples are consistent with the RTC samples only if the $VD_{PMF,opt}$ represents particle composition around the middle of the sample collection interval.~~

These results show that the particle composition measured after few hours of evaporation is consistent with the composition predicted based on composition observed at the start of evaporation and considering uncertainties of the interpreted C* values. The level of the agreement changes depending on which evaporation time the fresh FIGAERO-CIMS sample is assumed to represent. For medium O:C particles the VD_{PMF} and $VD_{PMF,opt}$ are more consistent when the fresh sample is assumed to represent particles at the maximum sample evaporation time. For low O:C particles the $VD_{PMF,opt}$ resembles the VD_{PMF} of the RTC sample best at mean evaporation time.

3.5 Volatility distribution comparison at dry condition

Next, we analyz~~s~~ed the evaporation experiments under dry conditions where the evaporation rate was reduced compared to the high RH conditions. We interpreted this difference as an indication of particle phase diffusion limitations at dry conditions (Yli-Juuti et al., 2017). Using the initial particle composition information obtained from the high RH experiments and the FIGAERO-CIMS data, we explored the effect of particle viscosity on the evaporation process. Our aim is to test if the slower evaporation, presumably due to higher viscosity of the SOA can be captured with a recently developed viscosity parametrization based on glass transition temperatures of various organic compounds (DeRieux et al., 2018). We also compare the results using the viscosity parametrization to an approach where we fit both the viscosity and VD to the evapogram.

First, we investigated the range of particle viscosities that are required to explain the observed slower evaporation at dry conditions. For this, we simulated the particle evaporation in dry conditions based only on the evapogram data. We used the VD_{evap} (i.e., the initial particle composition obtained by optimizing mole fractions of VD compounds with respect to the observed evapogram at high RH) as the initial condition for the simulations and optimized the b_i values (Eq. 3) for each VD compound. The best fit simulation from this optimization agrees well with the observed size decrease in the dry experiments for both low and medium O:C particles (Fig. 8, black line). Based on these simulations, the viscosity of the particles need to increase from below 10^5 Pa s to approximately 10^8 Pa s during the evaporation in order to explain the evaporation rate observed for the dry particles.

Second, we tested the performance of the composition dependent viscosity parameterization by DeRiuex et al. (2018) used together with the PMF results. For this, we calculated the volatility distribution, $VD_{PMF,dry}$, based on the T_{max} values of the factors from the fresh sample of the evaporation experiment at dry conditions (in the same way as VD_{PMF} for the high RH case). The mole fraction of each factor was calculated from the mass loading profile giving the initial mole fraction of each VD compound for the simulations. We assigned this $VD_{PMF,dry}$ as the particle composition at the mean evaporation time of the fresh sample, i.e. 15 minutes, and simulated the particle evaporation from there onward~~s~~. The particle size at the beginning of the simulation (i.e. at 15 minutes of evaporation) was taken from the above simulations optimized based only on the evapogram data, which fitted well ~~with~~to the measurements. We calculated the viscosity parameter b_i value for each VD compound as described in Section 2.5 based on the mass spectra of the factor and the parameterization by DeRieux et al. (2018). This resulted in too high viscosity for particles to evaporate in practice~~practise~~ at all during the length of the experiment for both low and medium O:C particles (grey~~black~~ dashed line in Fig. 8). Therefore, we also conducted ~~made~~ a simulation where the viscosity parameter b_i value for each factor was calculated based on the viscosity parameterization by setting the T_g values of all compounds 30 K lower than the parametrization predicted, which is in line with the uncertainties reported by DeRiuex et al. (2018). In this case, the simulated evaporation was faster than observed for medium O:C conditions (grey ~~dashed~~solid line in Fig. 8a) and similar to the evapogram calculated with VD_{evap} for low O:C conditions (grey solid line in Fig. 8b). This suggest that the observed evaporation rate at dry conditions and the viscosity parametrization by DeRieux et al. (2018) may be consistent with each other within the uncertainty range of the viscosity parametrization and the uncertainty range of the C^* of PMF factors.

Similar to Fig. 3, we show in Fig. 7 the comparison of $VD_{PMF,dry}$ (C^* from T_{max}) to the VD_{evap} at dry conditions and mean sample evaporation time with the VD compounds grouped into the three volatility classes. We show the mass loading profiles and the volatility distributions at dry conditions in Fig. S10~~5~~ and Fig. S11~~6~~. Figure S12 shows the same comparison as Fig 7 for other sample evaporation times. For medium O:C particles, $VD_{PMF,dry}$ calculated ~~both~~ from the fresh ~~and RTC~~ sample has~~ve~~ ~~slightly~~ more contribution of volatility classes 1 and ~~2 and~~ 3 and less of volatility class 2~~1~~ compared to the corresponding VD_{evap}. For low O:C particles, the $VD_{PMF,dry}$ of the fresh sample has more contribution of volatility class 3 and less of volatility classes 1 and 2 ~~differs substantially from~~ compared to the VD_{evap} ~~especially in the case of the fresh sample: considerably more matter is in the highest volatility class (class 3) than in the lowest volatility class (class 1)~~. ~~-~~ For medium O:C particles, the differences between the $VD_{PMF,dry}$ and VD_{evap} leave open the possibility that the underestimated evaporation rate calculated using $VD_{PMF,dry}$ is partly a result of inaccuracy in volatility description and not solely due to the high estimated viscosity. For low O:C particles the underestimated evaporation most likely stems from the high estimated viscosity since the $VD_{PMF,dry}$ is shifted towards higher volatility compounds than the VD_{evap}. ~~-dashed line in Fig. 8) originates from the high estimated viscosity. black Overall, the $VD_{PMF,dry}$ suggests higher volatility compared to the VD_{evap}. Therefore, the underestimation of the evaporation rate when using the $VD_{PMF,dry}$ together with the viscosity parameterization (~~

As a third investigation on the viscosity, we used again the PMF results of the fresh sample at dry conditions to initialize the particle composition in the model at the mean fresh sample evaporation time, i.e., at 15 minutes. ~~Also at this time, t~~The mole fraction of each factor was~~ere~~ calculated from the mass loading profile giving the initial mole fraction of each VD compound for the simulations similar to the high RH analysis. Then, using the MCGA algorithm together with the KM-GAP model, we estimated the b_i coefficient and C^* of each VD compound by optimizing the KM-GAP simulated evapogram to the measured evapogram at dry condition. This way we obtained both the initial volatility distribution ($VD_{PMF,dry,opt}$) and viscosity parameters b_i simultaneously. ~~-~~For this optimization, we restricted the C^* values of the factors based on the 25th and 75th percentile of the desorption temperature of the factors, similarly as done above for $VD_{PMF,opt}$, and the viscosity parameter b_i values based on the DeRieux et al. (2018) parameterization. The b_i values calculated with the original parametrization by DeRieux et al., (2018) were set as the upper limit for b_i values. The lower limit for b_i values were calculated by setting the glass transition temperature of each compound 30 K lower than the parametrization predicted. As above, also in these simulations the initial particle size was taken from the simulations where optimization was based on only the evapogram data. For both medium and low O:C particles it was possible to find a set of C^* and b_i values that produced an equally good match to experimental data as the VD_{evap} ~~produced~~ (purple and yellow lines in Fig. 8~~a~~). ~~For low O:C particles, the match to experimental data was slightly weaker than with the VD_{evap} (yellow line in Fig. 8b).~~

Figures 6b and 6d show~~s~~ the comparison of the measured and simulated particle composition, ~~on the basis of~~ grouped to the three volatility classes, at RTC sample collection time for the dry experiments for low and medium O:C particles. The measured composition is the VD calculated from the PMF results of the RTC sample at dry conditions.~~ and~~ T~~t~~he optimized C^* values of the factors from the corresponding dry experiment were used for these VD. The simulated particle composition is taken from the optimized model run (optimized $VD_{PMF,opt,dry}$ and b_i) at the mean RTC sample collection time similar to the high RH cases presented in Fig. 6a and Fig. 6c. ~~For medium O:C particles the measured and simulated composition at mean of the RTC collection time are in agreement.~~ For low O:C particles there is a clear discrepancy: the $VD_{PMF,opt}$~~measurements~~ imply a much larger relative contribution from the volatility classes 2~~1~~ and 3 and a smaller contribution from the volatility class 1~~2~~ compared to the measurements~~simulations~~. This inconsistency may be related to the rather high viscosities in the simulations. The viscosity of the low O:C particles in this optimized simulation was rather high, $\eta > 10^8$ Pa s, throughout the evaporation, slowing the evaporation of the higher volatility compounds. Similar evaporation curve could be obtained with lower viscosity and lower volatilities of the compounds.

4 Discussion

VD_{PMF} and $VD_{PMF,dry}$ capture qualitatively the evaporation dynamics well in all studied cases. For the VD_{PMF} of the fresh samples, the first and second factor desorb at low heating temperatures (below 100 °C) indicating that these factors represent high volatility organic compounds that evaporate almost completely from the particles in the experimental time scale of our isothermal evaporation experiments. In the RTC samples, these factors show significantly lower or non-existing signal strength relative to the other factors. The factors that desorb at high temperatures show an increase in the relative signal strength in the RTC samples compared to the fresh samples which is consistent with the expected increase in relative contribution of lower volatility compounds along evaporation. These findings indicate that the FIGAERO-CIMS measurements of α-pinene SOA and the applied PMF method give a good overall picture of the evolution of the volatility distribution during evaporation.

At high RH, the VD_{PMF} that was derived from T_{max} of each factors mass loading profile did not produce evapogram similar to the measured ones, when the VD_{PMF} was used as an input to the LLEVAP model. This reflects the sensitivity of particle evaporation to the C^* values and suggest that the VD_{PMF} is not directly applicable as a particle composition estimate for detailed particle dynamics study. When we allowed uncertainty in the C^* values of each factor we were able to explain most of the discrepancy between the simulated and measured evapograms. The simulated evapograms, after optimizing the C^* of each factor from their appropriate ranges, are close to the experimental values for~~at~~ all other cases except~~ n the low O:C casei~~ when the FIGAERO sample ~~VD$_{PMF}$~~is interpreted to represent particles at the start~~end~~ of fresh sample's collection interval (minimum~~maximum~~ evaporation time). Our results also demonstrate the need for careful investigation of the representative time of the sample when filter-collected samples are applied for dynamic processes such as evaporation.

In this study we assumed a quite large uncertainty range for the desorption temperature of each PMF factor and it is not certain that the determination of VD$_{PMF,opt}$ would be successful if the allowed ranges for C^* of PMF factors would be lower. Thus, there remains work to be done in studying what is the total uncertainty that rises from combining the FIGAERO-CIMS measurements with the PMF method and to what extent the PMF factors can be thought to represent surrogate organic compounds for the purpose of detailed SOA dynamics studies.

~~.Even though we assumed a quite large uncertainty range for the desorption temperature of each factor, the resulting C^* estimates range in most cases around one order of magnitude. In the cases where the C^* range is higher and a factor has high enough signal, the estimated C^* values in VD$_{PMF,opt}$ are closer to the C^* calculated from T$_{max}$ of the factor than the extremes of the range (e.g. factor 2 and factor 4 in medium O:C high RH experiments). This highlights the fact that even though the C^* estimated from T$_{max}$ did not produce exactly comparable evapograms, the C^* values that produce correct evaporation dynamics are not far away from those derived from the T$_{max}$ values~~

We note that care has to be taken when PMF results are transferred to volatility distributions, especially with regard to separating the contribution of instrument background and contamination from the true sample. When the sample mass was low (in the low O:C RTC sample) we noticed that the first half of the bimodal (factor LD1a) resulted in a high mole fraction even though the absolute signal strength of the factor did not change between the fresh and the RTC sample, which is usually an indication that this signal is caused by instrument background.~~ Factor LD1a affects the VD calculations only when the collected mass is low. Removing this factor from the low O:C RTC sample allowed us to derive VD$_{PMF,opt}$ that produces an evapogram similar to the experiment.~~ However, t~~T~~he signal strength of this factor was low enough in all~~ other~~ cases to not affect the overall VD estimation. More details on the interpretation of B- and D-type factors and potential factor blending can be found in Buchholz et al, (2019b)

At low RH, VD$_{PMF,dry}$ of the fresh sample in low O:C case showed noticeably higher amount of high volatility matter than VD$_{evap}$. ~~e cannot explain these differences with a single factor like in the low O:C high RH RTC sample case since in dry conditions multiple high volatility factors show up in the PMF solution.W~~ This discrepancy between the volatility distributions is not expected and raises a need for further studies on the role of viscosity and possible particle phase chemistry to SOA particle dynamics. Future studies should investigate the possibility of chemical reactions that modify the volatility of organic compounds and how viscosity is described in process models.

5 Conclusions

We compared volatility distributions derived from FIGAERO-CIMS measurements with PMF analysis to volatility distributions derived from fitting a process model to match measured size change of particles during isothermal evaporation. We compared the two methods for obtaining the volatility distribution data for two different particle compositions and two evaporation conditions. The results are promising and suggest that the methods provide volatility distributions that are in agreement. We note that the data set available here is limited and additional investigations on comparing the methods are desirable in the future.

In all studied experimental data sets we were able to capture the measured evaporation with the fitting method. With high RH experiments, VD_{PMF} deviated from VD_{evap} especially when the FIGAERO samples were collected at the early stages of the evaporation. However, qualitatively, both types of VD evolved similarly, i.e., the fraction of lower volatility compounds increased, and the fraction of higher volatility compounds decreased during the ~~particles'~~ evaporation of the particles. These results suggest that the changes in FIGAERO-CIMS derived volatility distributions over the isothermal evaporation are consistent with the observed isothermal evaporation and the detailed SOA dynamics are sensitive for the uncertainties in C^* values.

The volatility distribution from PMF at high RH agreed with the observed isothermal evaporation~~matched the experimental values~~ better when we interpreted the volatility of each factor as a range of possible C^* values and optimized the C^* values from these ranges with respect to the measurements. These results suggest that the FIGAERO-CIMS measurements combined with PMF method does not only provide qualitative information of the volatilities of the SOA constituents but it also has potential for quantitative investigation of the volatility distributions. However, more work is needed to constrain the uncertainties rising from the conversion of the FIGAEO-CIMS desorption temperatures to C^* values.

At dry conditions, we were able to simulate the evapograms based on the PMF results using the VTF equation and glass transition temperature parametrization of DeRieux et al., (2018) when both C^* and viscosity parameters where optimized and allowed to contain reasonable uncertainties. ~~For medium O:C particles also the simulated composition evolution was consistent with the measurements. However,~~ For both oxidation conditions ~~for low O:C particles~~ the measured composition at the later stages of evaporation suggested considerably lower~~higher~~ volatility than the simulations. These results suggest that the tested viscosity parameterization is not in disagreement with the observed SOA evaporation, however the uncertainties related to the method are significant from the point of view of simulating SOA dynamics.

Based on our analysis we conclude that using the PMF method with FIGAERO-CIMS thermogram data is good for estimating the volatility distribution of organic aerosols when the organic compounds present in the particle phase have low volatilities with respect to the sample collection and analysis time scale. Specifically, VD_{PMF} is useful for extracting information about organic compounds that do not evaporate during the evaporation measurements at room temperature. VD_{PMF} is applicable to detailed particle dynamics studies when desorption temperature of the factor is characterized with a range around the T_{max} value. Furthermore, combining $VD_{PMF,opt}$ with detailed process modelling and input optimization could allow quantification of other physical or chemical properties of organic aerosols since the FIGAERO-CIMS data constrains the particle composition and effectively decreases the search space that needs to be explored with global optimization methods.

Code availability: The process models ~~and the version of the MCGA~~ used in this study can be acquired upon request from the corresponding author. The MCGA code is can be obtained from https://doi.org/10.5281/zenodo.3759733

Author contributions: OPT, AB, SS, AV and TYJ designed the study. OPT did the calculations with support from AB and TYJ, except for the PMF calculations which were done by AB. AY developed the method to calculate C^* from desorption temperature with support from SS. All authors participated in the interpretation of the data. OPT wrote the paper with contributions from all co-authors.

Acknowledgments: The authors would like to thank Claudia Mohr and Wei Huang for the use of the FIGAERO instrument from the Karlsruhe Institute of Technology and their support during the FIGAERO-CIMS data analysis. Furthermore, we want to acknowledge Andrew Lambe and Aerodyne Research Inc. for lending us a Potential Aerosol Mass reactor.

Financial support: This work was supported by the Academy of Finland Center of Excellence programme (grant no. 307331), the Academy of Finland (project nos. 299544 and 310682), European Research Council (ERC StG QAPPA 335478) and the University of Eastern Finland Doctoral Program in Environmental Physics, Health and Biology.

Competing interests: The authors declare that they have no conflict of interest.

References

Angell, C. A.: Formation of glasses from liquids and biopolymers, Science, 267(5206), 1924–1935, 1995.

Angell, C. A.: Liquid Fragility and the Glass Transition in Water and Aqueous Solutions, Chem. Rev., 102(8), 2627–2650, doi:10.1021/cr000689q, 2002.

Bannan, T. J., Breton, M. L., Priestley, M., Worrall, S. D., Bacak, A., Marsden, N. A., Mehra, A., Hammes, J., Hallquist, M., Alfarra, M. R., Krieger, U. K., Reid, J. P., Jayne, J., Robinson, W., McFiggans, G., Coe, H., Percival, C. J. and Topping, D.: A method for extracting calibrated volatility information from the FIGAERO-HR-ToF-CIMS and its experimental application, Atmospheric Meas. Tech., 12(3), 1429–1439, doi:https://doi.org/10.5194/amt-12-1429-2019, 2019.

Berkemeier, T., Ammann, M., Krieger, U. K., Peter, T., Spichtinger, P., Pöschl, U., Shiraiwa, M. and Huisman, A. J.: Technical note: Monte Carlo genetic algorithm (MCGA) for model analysis of multiphase chemical kinetics to determine transport and reaction rate coefficients using multiple experimental data sets, Atmospheric Chem. Phys., 17(12), 8021–8029, doi:10.5194/acp-17-8021-2017, 2017.

Breton, M. L., Wang, Y., Hallquist, Å. M., Pathak, R. K., Zheng, J., Yang, Y., Shang, D., Glasius, M., Bannan, T. J., Liu, Q., Chan, C. K., Percival, C. J., Zhu, W., Lou, S., Topping, D., Wang, Y., Yu, J., Lu, K., Guo, S., Hu, M. and Hallquist, M.: Online gas- and particle-phase measurements of organosulfates, organosulfonates and nitrooxy organosulfates in Beijing utilizing a FIGAERO ToF-CIMS, Atmospheric Chem. Phys., 18(14), 10355–10371, doi:https://doi.org/10.5194/acp-18-10355-2018, 2018.

Buchholz, A., Ylisirniö, A., Huang, W., Mohr, C., Canagaratna, M., Worsnop, D. R., Schobesberger, S. and Virtanen, A.: Deconvolution of FIGAERO-CIMS thermal desorption profiles using positive matrix factorisation to identify chemical and physical processes during particle evaporation, Atmospheric Chem. Phys. Discuss., doi:https://doi.org/10.5194/acp-2019-926, 2019a.

Buchholz, A., Lambe, A. T., Ylisirniö, A., Li, Z., Tikkanen, O.-P., Faiola, C., Kari, E., Hao, L., Luoma, O., Huang, W., Mohr, C., Worsnop, D. R., Nizkorodov, S. A., Yli-Juuti, T., Schobesberger, S. and Virtanen, A.: Insights into the O:C-dependent mechanisms controlling the evaporation of α-pinene secondary organic aerosol particles, Atmospheric Chem. Phys., 19(6), 4061–4073, doi:10.5194/acp-19-4061-2019, 2019b.

Canagaratna, M. R., Jayne, J. T., Jimenez, J. L., Allan, J. D., Alfarra, M. R., Zhang, Q., Onasch, T. B., Drewnick, F., Coe, H., Middlebrook, A., Delia, A., Williams, L. R., Trimborn, A. M., Northway, M. J., DeCarlo, P. F., Kolb, C. E., Davidovits, P. and Worsnop, D. R.: Chemical and microphysical characterization of ambient aerosols with the aerodyne aerosol mass spectrometer, Mass Spectrom. Rev., 26(2), 185–222, doi:10.1002/mas.20115, 2007.

D’Ambro, E. L., Lee, B. H., Liu, J., Shilling, J. E., Gaston, C. J., Lopez-Hilfiker, F. D., Schobesberger, S., Zaveri, R. A., Mohr, C., Lutz, A., Zhang, Z., Gold, A., Surratt, J. D., Rivera-Rios, J. C., Keutsch, F. N. and Thornton, J. A.: Molecular composition and volatility of isoprene photochemical oxidation secondary organic aerosol under low- and high-NO_x conditions, Atmospheric Chem. Phys., 17(1), 159–174, doi:https://doi.org/10.5194/acp-17-159-2017, 2017.

D'Ambro, E. L., Schobesberger, S., Zaveri, R. A., Shilling, J. E., Lee, B. H., Lopez-Hilfiker, F. D., Mohr, C. and Thornton, J. A.: Isothermal Evaporation of α-Pinene Ozonolysis SOA: Volatility, Phase State, and Oligomeric Composition, ACS Earth Space Chem., 2(10), 1058–1067, doi:10.1021/acsearthspacechem.8b00084, 2018.

DeCarlo, P. F., Kimmel, J. R., Trimborn, A., Northway, M. J., Jayne, J. T., Aiken, A. C., Gonin, M., Fuhrer, K., Horvath, T., Docherty, K. S., Worsnop, D. R. and Jimenez, J. L.: Field-Deployable, High-Resolution, Time-of-Flight Aerosol Mass Spectrometer, Anal. Chem., 78(24), 8281–8289, doi:10.1021/ac061249n, 2006.

DeRieux, W.-S. W., Li, Y., Lin, P., Laskin, J., Laskin, A., Bertram, A. K., Nizkorodov, S. A. and Shiraiwa, M.: Predicting the glass transition temperature and viscosity of secondary organic material using molecular composition, Atmospheric Chem. Phys., 18(9), 6331–6351, doi:https://doi.org/10.5194/acp-18-6331-2018, 2018.

Dette, H. P., Qi, M., Schröder, D. C., Godt, A. and Koop, T.: Glass-Forming Properties of 3-Methylbutane-1,2,3-tricarboxylic Acid and Its Mixtures with Water and Pinonic Acid, J. Phys. Chem. A, 118(34), 7024–7033, doi:10.1021/jp505910w, 2014.

Donahue, N. M., Robinson, a. L., Stanier, C. O. and Pandis, S. N.: Coupled partitioning, dilution, and chemical aging of semivolatile organics, Environ. Sci. Technol., 40(8), 2635–2643, doi:10.1021/es052297c, 2006.

Gedeon, O.: Origin of glass fragility and Vogel temperature emerging from Molecular dynamics simulations, J. Non-Cryst. Solids, 498, 109–117, doi:10.1016/j.jnoncrysol.2018.06.012, 2018.

Glasius, M. and Goldstein, A. H.: Recent Discoveries and Future Challenges in Atmospheric Organic Chemistry, Environ. Sci. Technol., 50(6), 2754–2764, doi:10.1021/acs.est.5b05105, 2016.

Goldstein, A. H. and Galbally, I. E.: Known and Unexplored Organic Constituents in the Earth's Atmosphere, Environ. Sci. Technol., 41(5), 1514–1521, doi:10.1021/es072476p, 2007.

Hallquist, M., Wenger, J. C., Baltensperger, U., Rudich, Y., Simpson, D., Claeys, M., Dommen, J., Donahue, N. M., George, C., Goldstein, A. H., Hamilton, J. F., Herrmann, H., Hoffmann, T., Iinuma, Y., Jang, M., Jenkin, M. E., Jimenez, J. L., Kiendler-Scharr, A., Maenhaut, W., McFiggans, G., Mentel, Th. F., Monod, A., Prévôt, A. S. H., Seinfeld, J. H., Surratt, J. D., Szmigielski, R. and Wildt, J.: The formation, properties and impact of secondary organic aerosol: current and emerging issues, Atmos Chem Phys, 9(14), 5155–5236, doi:10.5194/acp-9-5155-2009, 2009.

Huang, W., Saathoff, H., Pajunoja, A., Shen, X., Naumann, K.-H., Wagner, R., Virtanen, A., Leisner, T. and Mohr, C.: α-Pinene secondary organic aerosol at low temperature: chemical composition and implications for particle viscosity, Atmos Chem Phys, 18(4), 2883–2898, doi:10.5194/acp-18-2883-2018, 2018.

Isaacman-VanWertz, G., Massoli, P., E. O'Brien, R., B. Nowak, J., R. Canagaratna, M., T. Jayne, J., R. Worsnop, D., Su, L., A. Knopf, D., K. Misztal, P., Arata, C., H. Goldstein, A. and H. Kroll, J.: Using advanced mass spectrometry techniques to fully characterize atmospheric organic carbon: current capabilities and remaining gaps, Faraday Discuss., 200(0), 579–598, doi:10.1039/C7FD00021A, 2017.

Isaacman-VanWertz, G., Massoli, P., O'Brien, R., Lim, C., Franklin, J. P., Moss, J. A., Hunter, J. F., Nowak, J. B., Canagaratna, M. R., Misztal, P. K., Arata, C., Roscioli, J. R., Herndon, S. T., Onasch, T. B., Lambe, A. T., Jayne, J. T., Su, L., Knopf, D. A., Goldstein, A. H., Worsnop, D. R. and Kroll, J. H.: Chemical evolution of atmospheric organic carbon over multiple generations of oxidation, Nat. Chem., 10(4), 462–468, doi:10.1038/s41557-018-0002-2, 2018.

Iyer, S., Lopez-Hilfiker, F., Lee, B. H., Thornton, J. A. and Kurtén, T.: Modeling the Detection of Organic and Inorganic Compounds Using Iodide-Based Chemical Ionization, J. Phys. Chem. A, 120(4), 576–587, doi:10.1021/acs.jpca.5b09837, 2016.

Jayne, J. T., Leard, D. C., Zhang, X., Davidovits, P., Smith, K. A., Kolb, C. E. and Worsnop, D. R.: Development of an Aerosol Mass Spectrometer for Size and Composition Analysis of Submicron Particles, Aerosol Sci. Technol., 33(1–2), 49–70, doi:10.1080/027868200410840, 2000.

Jimenez, J. L., Canagaratna, M. R., Donahue, N. M., Prevot, A. S. H., Zhang, Q., Kroll, J. H., DeCarlo, P. F., Allan, J. D., Coe, H., Ng, N. L., Aiken, A. C., Docherty, K. S., Ulbrich, I. M., Grieshop, A. P., Robinson, A. L., Duplissy, J., Smith, J. D., Wilson, K. R., Lanz, V. A., Hueglin, C., Sun, Y. L., Tian, J., Laaksonen, A., Raatikainen, T., Rautiainen, J., Vaattovaara, P., Ehn, M., Kulmala, M., Tomlinson, J. M., Collins, D. R., Cubison, M. J., Dunlea, E. J., Huffman, J. A., Onasch, T. B., Alfarra, M. R., Williams, P. I., Bower, K., Kondo, Y., Schneider, J., Drewnick, F., Borrmann, S., Weimer, S., Demerjian, K., Salcedo, D., Cottrell, L., Griffin, R., Takami, A., Miyoshi, T., Hatakeyama, S., Shimono, A., Sun, J. Y., Zhang, Y. M., Dzepina, K., Kimmel, J. R., Sueper, D., Jayne, J. T., Herndon, S. C., Trimborn, A. M., Williams, L. R., Wood, E. C., Middlebrook, A. M., Kolb, C. E., Baltensperger, U., Worsnop, D. R. and Worsnop, D. R.: Evolution of organic aerosols in the atmosphere., Science, 326(5959), 1525–9, doi:10.1126/science.1180353, 2009.

Kang, E., Root, M. J., Toohey, D. W. and Brune, W. H.: Introducing the concept of potential aerosol mass (PAM), Atmospheric Chem. Phys., 7(22), 5727–5744, 2007.

Lambe, A. T., Ahern, A. T., Williams, L. R., Slowik, J. G., Wong, J. P. S., Abbatt, J. P. D., Brune, W. H., Ng, N. L., Wright, J. P., Croasdale, D. R., Worsnop, D. R., Davidovits, P. and Onasch, T. B.: Characterization of aerosol photooxidation flow reactors: heterogeneous oxidation, secondary organic aerosol formation and cloud condensation nuclei activity measurements, Atmospheric Meas. Tech., 4(3), 445–461, doi:10.5194/amt-4-445-2011, 2011.

Lee, B. H., Lopez-Hilfiker, F. D., Mohr, C., Kurtén, T., Worsnop, D. R. and Thornton, J. A.: An Iodide-Adduct High-Resolution Time-of-Flight Chemical-Ionization Mass Spectrometer: Application to Atmospheric Inorganic and Organic Compounds, Environ. Sci. Technol., 48(11), 6309–6317, doi:10.1021/es500362a, 2014.

Lee, B. H., Lopez-Hilfiker, F. D., D'Ambro, E. L., Zhou, P., Boy, M., Petäjä, T., Hao, L., Virtanen, A. and Thornton, J. A.: Semi-volatile and highly oxygenated gaseous and particulate organic compounds observed above a boreal forest canopy, Atmospheric Chem. Phys., 18(15), 11547–11562, doi:https://doi.org/10.5194/acp-18-11547-2018, 2018.

Lehtinen, K. E. J. and Kulmala, M.: A model for particle formation and growth in the atmosphere with molecular resolution in size, Atmos Chem Phys, (3), 251–257, doi:https://doi.org/10.5194/acp-3-251-2003, 2003.

Lopez-Hilfiker, F. D., Mohr, C., Ehn, M., Rubach, F., Kleist, E., Wildt, J., Mentel, Th. F., Lutz, A., Hallquist, M., Worsnop, D. and Thornton, J. A.: A novel method for online analysis of gas and particle composition: description and evaluation of a Filter Inlet for Gases and AEROsols (FIGAERO), Atmospheric Meas. Tech., 7(4), 983–1001, doi:10.5194/amt-7-983-2014, 2014.

Lopez-Hilfiker, F. D., Mohr, C., Ehn, M., Rubach, F., Kleist, E., Wildt, J., Mentel, T. F., Carrasquillo, A. J., Daumit, K. E., Hunter, J. F., Kroll, J. H., Worsnop, D. R. and Thornton, J. A.: Phase partitioning and volatility of secondary organic aerosol components formed from α-pinene ozonolysis and OH oxidation: the importance of accretion products and other low volatility compounds, Atmospheric Chem. Phys., 15(14), 7765–7776, doi:https://doi.org/10.5194/acp-15-7765-2015, 2015.

Lopez-Hilfiker, F. D., Mohr, C., D’Ambro, E. L., Lutz, A., Riedel, T. P., Gaston, C. J., Iyer, S., Zhang, Z., Gold, A., Surratt, J. D., Lee, B. H., Kurten, T., Hu, W. W., Jimenez, J., Hallquist, M. and Thornton, J. A.: Molecular Composition and Volatility of Organic Aerosol in the Southeastern U.S.: Implications for IEPOX Derived SOA, Environ. Sci. Technol., 50(5), 2200–2209, doi:10.1021/acs.est.5b04769, 2016.

Paatero, P. and Tapper, U.: Positive matrix factorization: A non-negative factor model with optimal utilization of error estimates of data values, Environmetrics, 5(2), 111–126, doi:10.1002/env.3170050203, 1994.

Pathak, R. K., Presto, A. A., Lane, T. E., Stanier, C. O., Donahue, N. M. and Pandis, S. N.: Ozonolysis of α-pinene: parameterization of secondary organic aerosol mass fraction, Atmospheric Chem. Phys., 7(14), 3811–3821, doi:10.5194/acp-7-3811-2007, 2007.

Reid, J. P., Bertram, A. K., Topping, D. O., Laskin, A., Martin, S. T., Petters, M. D., Pope, F. D. and Rovelli, G.: The viscosity of atmospherically relevant organic particles, Nat. Commun., 9(1), 956, doi:10.1038/s41467-018-03027-z, 2018.

Reid, R. C., Prausnitz, J. M. and Poling, B. E.: The properties of gases and liquids, 1987.

Renbaum-Wolff, L., Grayson, J. W., Bateman, A. P., Kuwata, M., Sellier, M., Murray, B. J., Shilling, J. E., Martin, S. T. and Bertram, A. K.: Viscosity of α-pinene secondary organic material and implications for particle growth and reactivity, Proc. Natl. Acad. Sci., 110(20), 8014–8019, doi:10.1073/pnas.1219548110, 2013.

Schobesberger, S., D&apos;Ambro, E. L., Lopez-Hilfiker, F. D., Mohr, C. and Thornton, J. A.: A model framework to retrieve thermodynamic and kinetic properties of organic aerosol from composition-resolved thermal desorption measurements, Atmospheric Chem. Phys. Discuss., 1–50, doi:10.5194/acp-2018-398, 2018.

Shiraiwa, M., Pfrang, C., Koop, T. and Pöschl, U.: Kinetic multi-layer model of gas-particle interactions in aerosols and clouds (KM-GAP): linking condensation, evaporation and chemical reactions of organics, oxidants and water, Atmospheric Chem. Phys., 12(5), 2777–2794, doi:10.5194/acp-12-2777-2012, 2012.

Shiraiwa, M., Li, Y., Tsimpidi, A. P., Karydis, V. A., Berkemeier, T., Pandis, S. N., Lelieveld, J., Koop, T. and Pöschl, U.: Global distribution of particle phase state in atmospheric secondary organic aerosols, Nat. Commun., 8, 15002, doi:10.1038/ncomms15002, 2017.

Stark, H., Yatavelli, R. L. N., Thompson, S. L., Kang, H., Krechmer, J. E., Kimmel, J. R., Palm, B. B., Hu, W., Hayes, P. L., Day, D. A., Campuzano-Jost, P., Canagaratna, M. R., Jayne, J. T., Worsnop, D. R. and Jimenez, J. L.: Impact of Thermal

Decomposition on Thermal Desorption Instruments: Advantage of Thermogram Analysis for Quantifying Volatility Distributions of Organic Species, , doi:10.1021/acs.est.7b00160, 2017.

Stocker, T. F., Qin, D., Plattner, G.-K., Tignor, M., Allen, S. K., Boschung, J., Nauels, A., Xia, Y., Bex, V., Midgley, P. M. and others: Climate change 2013: The physical science basis, Cambridge University Press Cambridge., 2013.

Tikkanen, O.-P., Hämäläinen, V., Rovelli, G., Lipponen, A., Shiraiwa, M., Reid, J. P., Lehtinen, K. E. J. and Yli-Juuti, T.: Optimization of process models for determining volatility distribution and viscosity of organic aerosols from isothermal particle evaporation data, Atmospheric Chem. Phys., 19(14), 9333–9350, doi:https://doi.org/10.5194/acp-19-9333-2019, 2019.

Vaden, T. D., Imre, D., Beránek, J., Shrivastava, M. and Zelenyuk, A.: Evaporation kinetics and phase of laboratory and ambient secondary organic aerosol., Proc. Natl. Acad. Sci. U. S. A., 108(6), 2190–2195, doi:10.1073/pnas.1013391108, 2011.

Vesala, T., Kulmala, M., Rudolf, R., Vrtala, A. and Wagner, P. E.: Models for condensational growth and evaporation of binary aerosol particles, J. Aerosol Sci., 28(4), 565–598, doi:10.1016/S0021-8502(96)00461-2, 1997.

Virtanen, A., Joutsensaari, J., Koop, T., Kannosto, J., Yli-Pirilä, P., Leskinen, J., Mäkelä, J. M., Holopainen, J. K., Pöschl, U., Kulmala, M., Worsnop, D. R. and Laaksonen, A.: An amorphous solid state of biogenic secondary organic aerosol particles, Nature, 467(7317), 824–827, doi:10.1038/nature09455, 2010.

Wilson, J., Imre, D., Beraek, J., Shrivastava, M. and Zelenyuk, A.: Evaporation Kinetics of Laboratory-Generated Secondary Organic Aerosols at Elevated Relative Humidity, Environ. Sci. Technol., 49(1), 243–249, doi:10.1021/es505331d, 2015.

Yli-Juuti, T., Pajunoja, A., Tikkanen, O.-P., Buchholz, A., Faiola, C., Väisänen, O., Hao, L., Kari, E., Peräkylä, O., Garmash, O., Shiraiwa, M., Ehn, M., Lehtinen, K. and Virtanen, A.: Factors controlling the evaporation of secondary organic aerosol from α-pinene ozonolysis, Geophys. Res. Lett., 44(5), 2016GL072364, doi:10.1002/2016GL072364, 2017.

Zhang, Q., Alfarra, M. R., Worsnop, D. R., Allan, J. D., Coe, H., Canagaratna, M. R. and Jimenez, J. L.: Deconvolution and Quantification of Hydrocarbon-like and Oxygenated Organic Aerosols Based on Aerosol Mass Spectrometry, Environ. Sci. Technol., 39(13), 4938–4952, doi:10.1021/es048568l, 2005.

Zhang, Q., Jimenez, J. L., Canagaratna, M. R., Allan, J. D., Coe, H., Ulbrich, I., Alfarra, M. R., Takami, A., Middlebrook, A. M., Sun, Y. L., Dzepina, K., Dunlea, E., Docherty, K., DeCarlo, P. F., Salcedo, D., Onasch, T., Jayne, J. T., Miyoshi, T., Shimono, A., Hatakeyama, S., Takegawa, N., Kondo, Y., Schneider, J., Drewnick, F., Borrmann, S., Weimer, S., Demerjian, K., Williams, P., Bower, K., Bahreini, R., Cottrell, L., Griffin, R. J., Rautiainen, J., Sun, J. Y., Zhang, Y. M. and Worsnop, D. R.: Ubiquity and dominance of oxygenated species in organic aerosols in anthropogenically-influenced Northern Hemisphere midlatitudes, Geophys. Res. Lett., 34(13), doi:10.1029/2007GL029979, 2007.

Zhang, Q., Jimenez, J. L., Canagaratna, M. R., Ulbrich, I. M., Ng, N. L., Worsnop, D. R. and Sun, Y.: Understanding atmospheric organic aerosols via factor analysis of aerosol mass spectrometry: a review, Anal. Bioanal. Chem., 401(10), 3045–3067, doi:10.1007/s00216-011-5355-y, 2011.

Table 1: The ambient conditions and properties of the organic compounds used in estimating the VD_{evap}. The variables are, from top to bottom, temperature (T) during the evaporation, relative humidity (RH), gas phase diffusion coefficient ($D_{g,org}$), molar mass (M), particle phase density (ρ), particle surface tension (σ) and mass accommodation coefficient (α). Rows that only have one value are the same in every column.

Variable	Medium O:C High RH	Low O:C High RH	Medium O:C dry	Low O:C dry
T (K)	293.85	293.75	293.75	293.35
RH (%)	82.4	83.5	0	0
$D^{a,b}_{gas}$ ($cm^2\ s^{-1}$)	0.05			
	~~0.05~~			
	~~0.05~~			
	~~0.05~~			
M^{b} ($g\ mol^{-1}$)	200			
	~~200~~			
	~~200~~			
	~~200~~			
ρ^{b} ($kg\ m^{-3}$)	1200			
	~~1200~~			
	~~1200~~			
	~~1200~~			
σ^{b} ($mN\ m^{-1}$)	40			
	~~40~~			
	~~40~~			
	~~40~~			
α^{b}	1			
	~~1~~			
	~~1~~			
	~~1~~			

[a] The gas phase diffusion coefficients are scaled to correct temperatures by multiplying with a factor of $(T/273.15)^{1.75}$ (Reid et al., 1987)

[b] values are chosen to represent a generic organic compound with values similar to other α-pinene SOA studies (e.g. Pathak et al., 2007; Vaden et al., 2011; Yli-Juuti et al., 2017).

~~**Table 2:** Minimum, mean and maximum time that the particles have evaporated during the FIGAERO sample collection. All times are relative to the start of RTC filling.~~

~~Sample~~	~~Minimum evaporation time (min)~~	~~Mean evaporation time (min)~~	~~Maximum evaporation time (min)~~
~~Medium O:C high RH fresh~~	~~0~~	~~15~~	~~30~~
~~Medium O:C high RH RTC~~	~~173~~	~~216~~	~~259~~
~~Medium O:C dry fresh~~	~~0~~	~~15~~	~~30~~
~~Medium O:C dry RTC~~	~~170~~	~~213~~	~~256~~
~~Low O:C high RH fresh~~	~~0~~	~~15~~	~~30~~
~~Low O:C high RH RTC~~	~~168~~	~~211~~	~~254~~
~~Low O:C dry fresh~~	~~0~~	~~15~~	~~30~~
~~Low O:C dry RTC~~	~~152~~	~~195~~	~~238~~

Table 2~~3~~: The best fit C^* values for medium O:C and low O:C high RH experiments when C^* values of PMF factors were optimized with respect to the measured isothermal evaporation. C^* values were optimized by assuming the FIGAERO-CIMS sample represents particle composition at the mean sample evaporation time for the fresh sample and the minimum sample evaporation time for the RTC sample.~~For each experiment three different results are given which correspond to simulations initialized with the PMF mole fraction at the minimum, mean and maximum time that the particles have evaporated during the sample collection (See Table 2).~~ The C^* values are rounded to two significant digits and are in units μgm^{-3}. C^* values below 10^{-3} μgm^{-3} are not reported explicitly since the evapogram fitting method is not sensitive to these values.

	~~Medium O:C fresh sample min evap. time~~	Medium O:C fresh sample ~~mean evap. time~~	~~Medium O:C fresh sample max evap. time~~	Medium O:C RTC sample ~~min evap time~~	~~Low O:C fresh sample min evap. time~~	Low O:C fresh sample ~~mean evap. time~~	~~Low O:C fresh sample max evap. time~~	Low O:C RTC sample ~~min evap time~~
Factor M1/L1	~~$9.79 \cdot 10^{-1}$~~	$4.96 \cdot 10^{-1}$ ~~$5.36 \cdot 10^{-1}$~~	~~$3.07 \cdot 10^{-1}$~~	36.10 ~~$3.06 \cdot 10^{-1}$~~	~~$9.76 \cdot 10^{-1}$~~	$3.06 \cdot 10^{-1}$ ~~$1.92 \cdot 10^{-1}$~~	~~$1.92 \cdot 10^{-1}$~~	$<10^{-3}$
Factor M2/L2	~~6.10~~	$2.89 \cdot 10^{-1}$ ~~$2.32 \cdot 10^{-1}$~~	~~$7.01 \cdot 10^{-2}$~~	$4.12 \cdot 10^{-1}$ ~~$9.41 \cdot 10^{-2}$~~	~~12.61~~	$3.55 \cdot 10^{-1}$ ~~$7.98 \cdot 10^{-1}$~~	~~$8.15 \cdot 10^{-1}$~~	$2.40 \cdot 10^{-2}$ ~~$1.65 \cdot 10^{-1}$~~
Factor M3/L3	~~$1.68 \cdot 10^{-1}$~~	$9.93 \cdot 10^{-3}$ ~~$2.37 \cdot 10^{-2}$~~	~~$9.49 \cdot 10^{-3}$~~	$4.42 \cdot 10^{-3}$ ~~$9.50 \cdot 10^{-2}$~~	~~$2.90 \cdot 10^{-1}$~~	$2.87 \cdot 10^{-2}$ ~~$2.57 \cdot 10^{-2}$~~	~~$2.48 \cdot 10^{-2}$~~	$7.13 \cdot 10^{-3}$ ~~$7.32 \cdot 10^{-2}$~~
Factor M4/L4	~~$1.39 \cdot 10^{-2}$~~	$< 10^{-3}$	~~$< 10^{-3}$~~	$< 10^{-3}$	~~$5.52 \cdot 10^{-2}$~~	$1.54 \cdot 10^{-3}$ ~~$2.65 \cdot 10^{-3}$~~	~~$2.65 \cdot 10^{-3}$~~	$< 10^{-3}$ ~~$2.14 \cdot 10^{-2}$~~
Factor M5/L5	~~$< 10^{-3}$~~	$< 10^{-3}$	~~$< 10^{-3}$~~	$< 10^{-3}$	~~$1.14 \cdot 10^{-2}$~~	$< 10^{-3}$ ~~$1.55 \cdot 10^{-3}$~~	~~$< 10^{-3}$~~	$< 10^{-3}$ ~~$7.33 \cdot 10^{-3}$~~
Factor D1a	~~70.14~~	$7.68 \cdot 10^{-1}$ ~~10.86~~	~~$1.67 \cdot 10^{-2}$~~	69.35 ~~11.82~~	~~59.73~~	130.03 ~~$7.48 \cdot 10^{-1}$~~	~~$7.34 \cdot 10^{-1}$~~	$1.04 \cdot 10^{-1}$ ~~/~~
Factor D1b	~~$< 10^{-3}$~~	$< 10^{-3}$	~~$< 10^{-3}$~~	$< 10^{-3}$	~~$< 10^{-3}$~~	$< 10^{-3}$	~~$< 10^{-3}$~~	$< 10^{-3}$

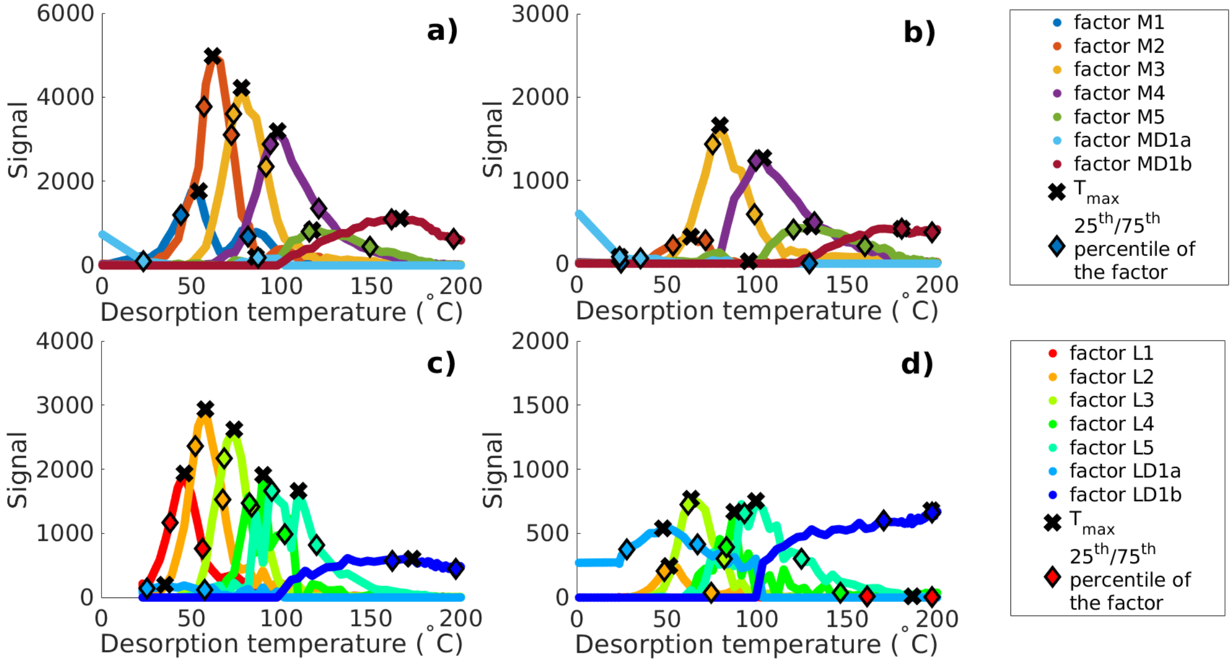

Figure 1: Main positive matrix factorization (PMF) mass loading profiles for thermal desorption of secondary organic aerosol (SOA) from α-pinene at high RH conditions

a) Fresh sample of medium O:C SOA ~~, samplefresh~~

b) Residual particles of medium O:C SOA after 173-259 minutes of evaporation in a residence time chamber (RTC), i.e., the RTC sample ~~,sampleRTC~~

c) Fresh sample of low O:C SOA ~~sample,fresh~~

d) Residual particles of low O:C SOA after 168-254 minutes of evaporation in the RTC, i.e. the RTC sample~~-.RTC sample.~~

Black crosses indicate the peak desorption temperature T_{max} and the diamonds mark the 25th and 75th percentiles of each ~~the~~ factor's area.

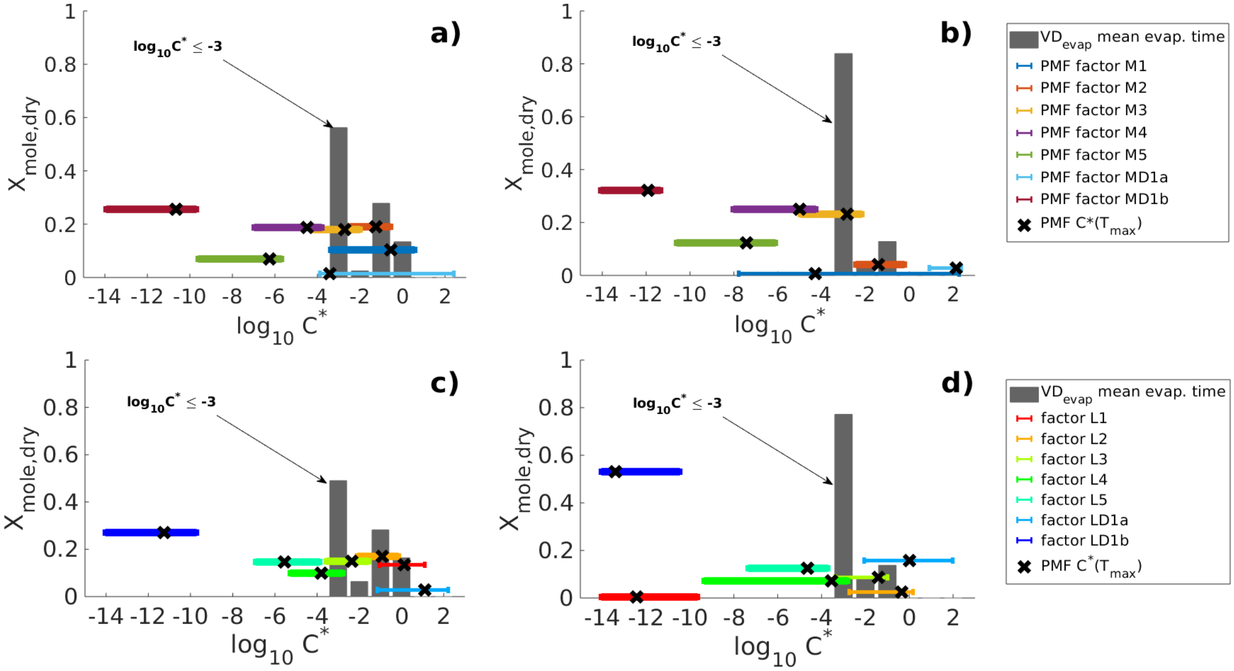

Figure 2: Volatility distributions in high RH experiments determined from model fitting (VD$_{evap}$) and PMF analysis ~~(VD$_{PMF}$)~~ of~~n~~ FIGAERO-CIMS data (VD$_{PMF}$) for the same four cases shown in Fig. 1.

~~-~~a) Fresh sample of medium O:C SOA ~~, samplefresh~~

b) Residual particles of medium O:C SOA (the RTC sample)~~, sampleRTC~~

c) Fresh sample of low O:C SOA~~, samplefresh~~

d) Residual particles of low O:C SOA (the RTC sample).~~RTC sample.~~

VD$_{evap}$ is shown for the best fit simulation (grey bars) at the mean evaporation time of the FIGAERO-CIMS sample. ~~The different grey shades show the VD$_{evap}$ in the simulation at minimum, mean and maximum time that the particles have evaporated when the FIGAERO sample was collected (see Table 2).~~ Black crosses show the log$_{10}$(C*) calculated for each PMF factor from the peak desorption temperature T$_{max}$. The horizontal coloured lines show the range of log$_{10}$(C*) calculated from the 25th and 75th percentiles of each PMF factor's mass loading profile.

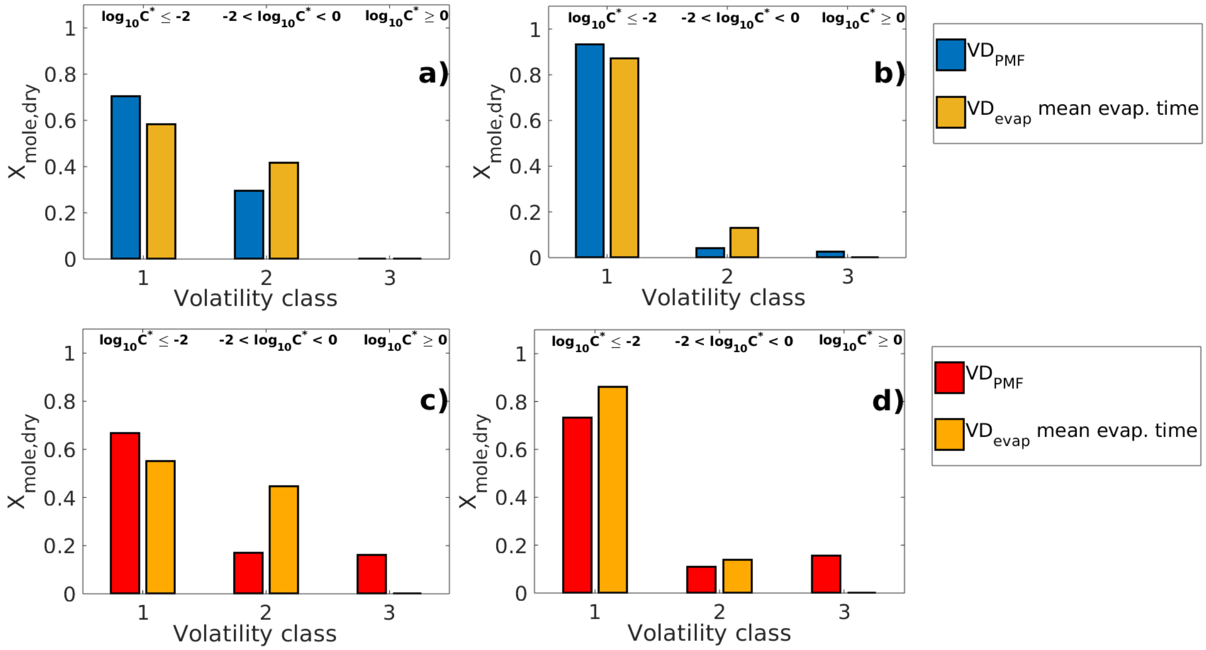

Figure 3: Comparison of VD_{PMF} and VD_{evap} at mean sample evaporation time in high RH experiments for the same four cases shown in Fig. 1.

a) Fresh sample of medium O:C SOA

b) Residual particles of medium O:C SOA (the RTC sample)

c) Fresh sample of low O:C SOA

d) Residual particles of low O:C SOA (the RTC sample). ~~.~~

The VD compounds shown in Fig. 2 are grouped into three different volatility classes based on their evaporation tendency with respect to the measurement time scale and particle size. The limits for each volatility class are shown at the top and are the same for each subfigure. The VD_{PMF} shows lower overall volatility than the VD_{evap} except for subfigure d (RTC sample of low O:C SOA) where the VD_{PMF} shows higher overall volatility than the VD_{evap}. ~~a) medium O:C fresh sample, b) medium O:C RTC sample, c) low O:C fresh sample, d) low O:C RTC sample.: log(C^*) ≤ -2, 2: -2 < log(C^*) < 0, 3: log(C^*) > 0. The volatility classes are 1Min, mean and max evaporation time refer to the FIGAERO sample collection times presented in Table 2..~~

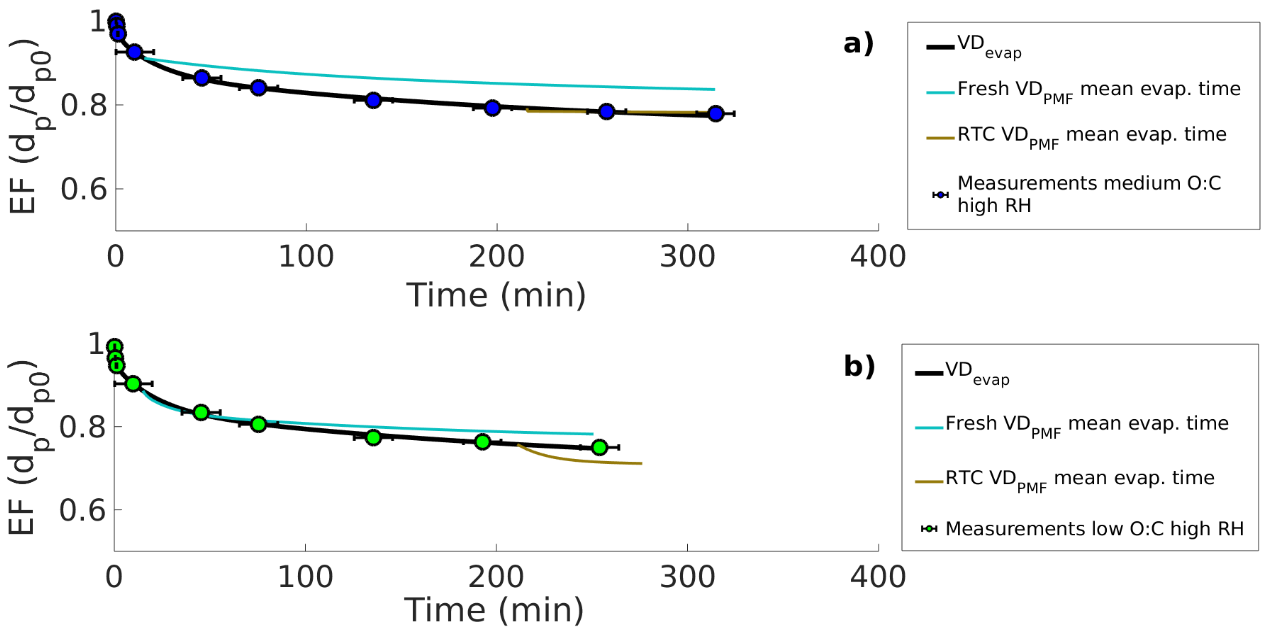

Figure 4: Evapograms of high RH experiments showing the ~~high RH measured~~ evaporation factors (remaining fraction of the initial particle diameter; circles) and their uncertainty in time for a) medium O:C SOA and b) low O:C SOA, ~~and their uncertainty in time,~~ LLEVAP simulated evapograms calculated using the best fit VD_{evap} (black solid lines) and LLEVAP simulated evapograms calculated with VD_{PMF} (turquoise ~~solid~~ lines for VD_{PMF} of fresh SOA ~~sample~~ and light brown ~~solid~~ lines for simulations with VD_{PMF} of the residual particles evaporated 173-259 minutes and 168-254 minutes for medium O:C and low O:C SOA, respectively)~~sampleRTC _ a) medium O:C b) low O:C.~~. The evapograms calculated with VD_{PMF} of fresh SOA show lower rate of evaporation than the evapogram calculated with VD_{evap} consistent with volatility distribution shown in Fig. 3. The evapograms calculated with VD_{PMF} of the residual particles (the RTC sample) show similar rate of evaporation for medium O:C SOA and faster rate of evaporation for low O:C SOA compared to evapograms calculated with VD_{evap} similarly consistent with Fig. 3.

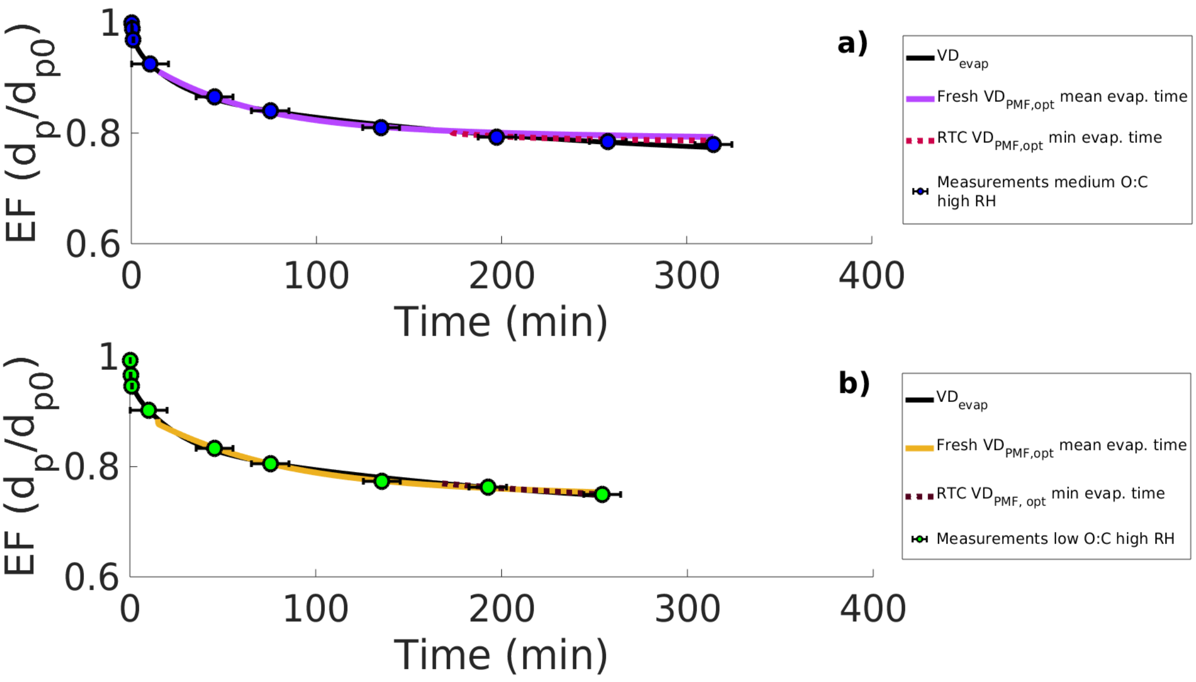

Figure 5: Evapograms of high RH experiments showing the ~~high RH measured~~ evaporation factors (circles), ~~and~~ their uncertainty in time (black whiskers), ~~and~~ the best fit simulated evapogram calculated with VD_{evap} (black solid line) and~~.~~ ~~Other lines show~~ the best fit simulated evapograms calculated with the volatility distribution where the effective saturation concentration (C^*) of each PMF factors are fitted to the measurements ($VD_{PMF,opt}$). ~~a) medium O:C, b) low O:C.~~

a) Medium O:C SOA

b) Low O:C SOA.

The colored solid lines are for the fresh SOA and the dashed lines for the residual particles collected from the RTC after 173-259 minutes and 168-254 minutes of evaporation for medium O:C and low O:C SOA, respectively. For fitting, the C^* of each PMF factor were allowed values from their respective 25th and 75th percentile desorption temperature shown in Fig. 1.

All the evapograms calculated with the $VD_{PMF,opt}$ match the measured evaporation highlighting that the volatility distribution determined from the FIGAERO-CIMS data with the PMF method can describe the dynamics of evaporating SOA particles when uncertainties in the C^* of the factors are considered.

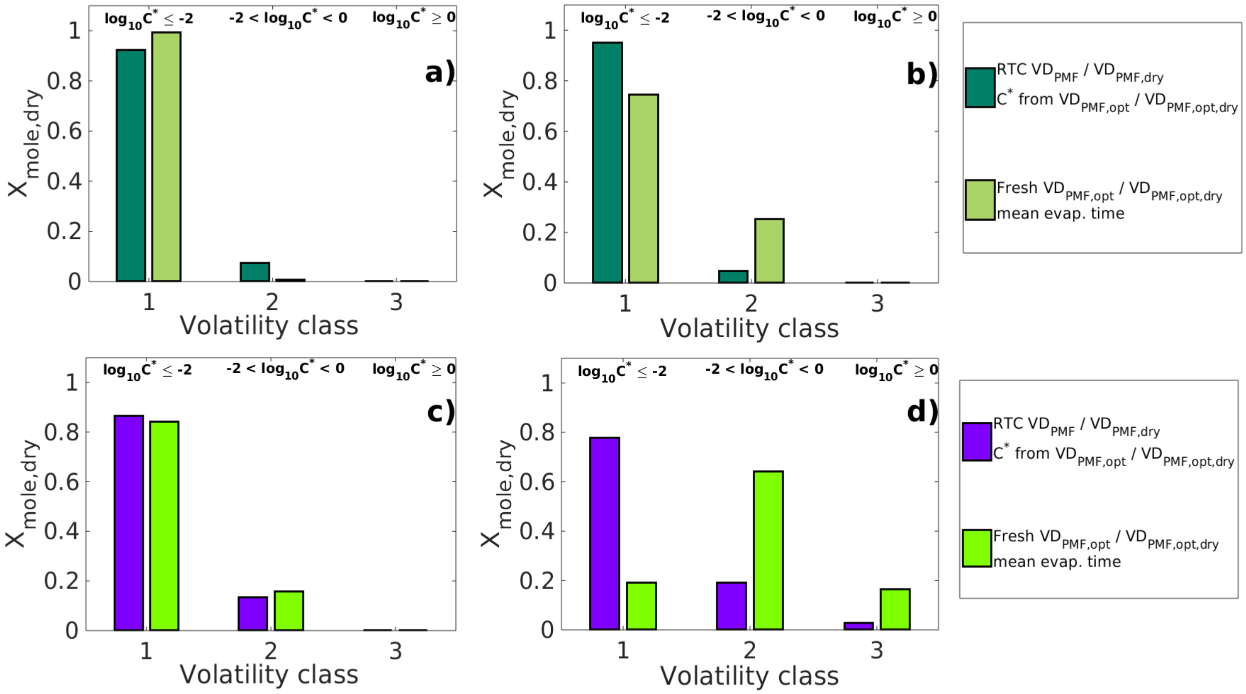

Figure 6: Comparison of the simulated particle composition ($VD_{PMF,opt}$, $VD_{PMF,opt,dry}$) to the particle composition determined from the residual particles collected from the RTC ($VD_{PMF}/VD_{PMF,dry}$) after 173-259 minutes and 168-254 minutes of evaporation for medium O:C and low O:C SOA, respectively. The simulated compositions (~~-~~$VD_{PMF,opt}$ in a and c, ~~-(~~$VD_{PMF,opt,dry}$ ~~for subfigures~~in b and d~~e~~) are taken from the best fit simulated evapogram obtained from the optimization of the C^* values of fresh sample PMF factors to measured evapogram. The volatility of individual VD compounds are grouped into three volatility classes similar to Fig. 3. The limits for each volatility class are shown at the top and are the same for each subfigure. The C^* values from $VD_{PMF,opt}/VD_{PMF,opt,dry}$ were used for corresponding $VD_{PMF}/VD_{PMF,dry}$ when the volatility grouping was calculated in order to ensure the comparability.

a) Medium O:C SOA in high RH experiment

b) Medium O:C SOA in low RH experiment

c) Low O:C SOA in high RH experiment

d) Low O:C SOA in low RH experiment.

In the high RH cases (sugfigures a and c) the volatility distributions simulated based on $VD_{PMF,opt}$ of the fresh SOA are similar to the measured $VD_{PMF,}$ while for the low RH cases (subfigures b and d) the volatility distributions simulated based on $VD_{PMF,opt,dry}$ show higher volatility than the measured VD_{PMF}.~~The subscripts min, mean and max refer to the points from the fresh sample collection interval from where the $VD_{PMF,opt}$ simulations were initialised (see Table 2) collection interval of the RTC sample. time of the) of RTC samples at the mean cof the fresh samples to VD_{PMF} ($VD_{PMF,dry}$ for subfigures b and~~ . ~~a) medium OC high RH samples, b) medium O:C low RH samples, c) low O:C high RH samples d) low O:C low RH samples.The volatility classes are 1: log(C^*) ≤ -2, 2: -2 < log(C^*) < 0, 3: log(C^*) > 0.~~

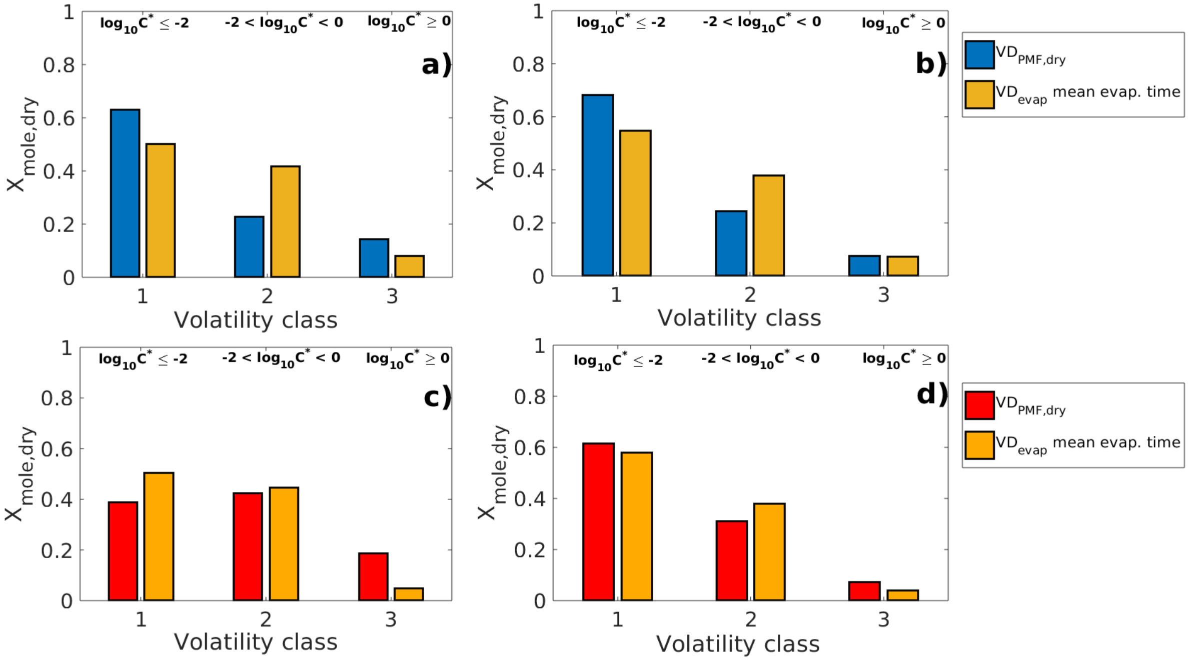

Figure 7: Comparison of VD$_{PMF,dry}$ (volatility distribution where C* is calculated from the peak desorption temperature, T$_{max}$, of each PMF factor) and VD$_{evap}$ (volatility distribution determined by fitting LLEVAP model to measured evapogram) at mean evaporation time of the SOA samples in dry condition experiments. The VD compounds are grouped into three different volatility classes similar to Fig. 3. The limits for each volatility class are shown at the top and are the same for each subfigure.

a) Fresh sample of medium O:C SOA

b) Residual particles of medium O:C SOA after 170-256 minutes of evaporation (the RTC sample)

c) Fresh sample of low O:C SOA

d) Residual particles of low O:C SOA after 152-238 minutes of evaporation (the RTC sample).

The VD$_{PMF,dry}$ shows lower overall volatility than the VD$_{evap}$ for medium O:C SOA. For low O:C SOA the VD$_{PMF,dry}$ shows higher volatility for fresh sample and similar volatility compared to VD$_{evap}$ after 152-238 minutes of evaporation. ~~a) medium O:C fresh sample, b) medium O:C RTC sample, c) low O:C fresh sample, d) low O:C RTC sample. 1: log(C*) ≤ -2, 2: -2 < log(C*) < 0, 3: log(C*) > 0. The volatility classes areMin, mean and max evaporation time refer to the FIGAERO sample collection times presented in Table 2. .he VD compounds are grouped into three volatility classes where t~~

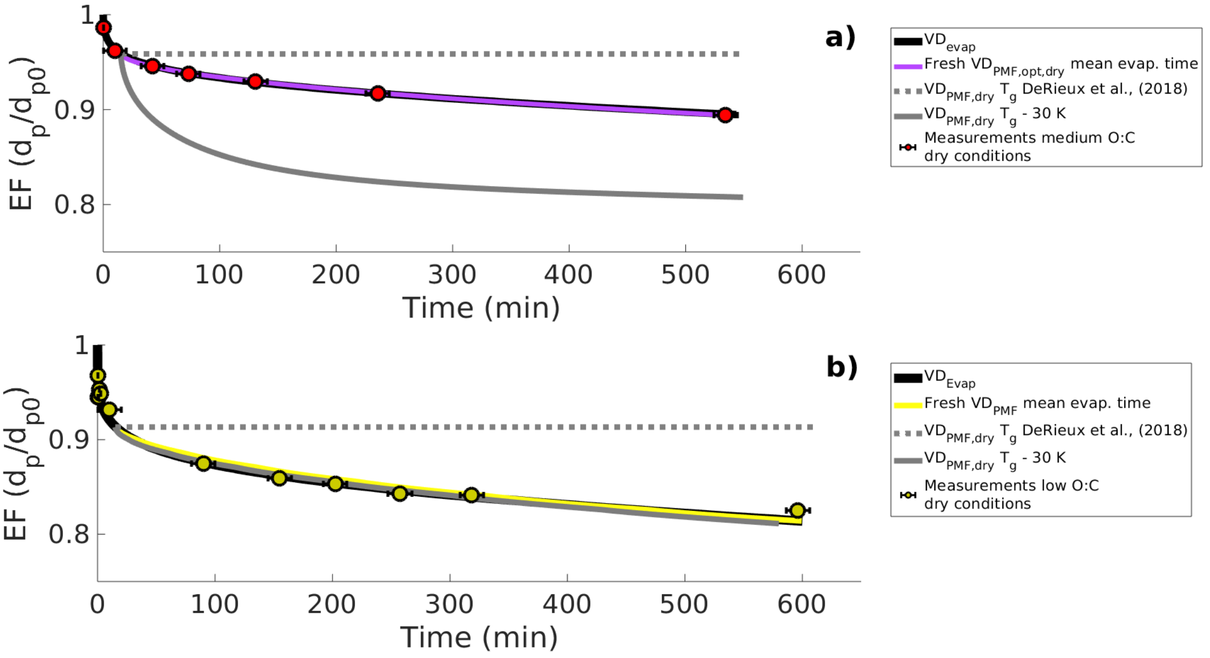

Figure 8: Evapograms showing the measured isothermal evaporation of a) medium O:C SOA~~particles~~ b) low O:C SOA ~~particles~~ in~~at~~ dry condition experiments~~s~~ and their uncertainty in time (red and yellow markers and black whiskers) together with the simulated evapograms. ~~and t~~The best fit simulated evapogram calculated with VD$_{evap}$ (obtained from high RH experiments) and optimizing b$_i$ is shown with ~~(~~black solid line~~).~~. ~~.(see Table 2)Purple and yellow solid lines show the best fit simulated evapograms calculated with VD$_{PMF,opt,dry}$ assuming that the FIGAERO sample represents particles at mean of the sample collection interval. Black and~~ Ggrey ~~dashed~~ lines show the minimum and maximum possible evaporation calculated with VD$_{PMF,dry}$ (C* of PMF factors calculated from T$_{max}$) and the highest (the original parametrization of DeRieux et al., (2018), grey dashed lines) or the lowest (30 K subtracted from the T$_g$ of every ion, grey solid line) studied viscosity. Purple and yellow solid lines show the best fit simulated evapograms calculated with the optimized VD$_{PMF,opt,dry}$ (based on the assumption that the FIGAERO sample represents particles at the mean of the sample collection interval) and b$_i$ restricted based on the DeRieux et al. (2018) parameterization. The figure shows, similar to Fig. 5, that the volatility distribution determined from the FIGAERO-CIMS data with the PMF method is consistent with the measured evaporation of the SOA particles once the uncertainty in the effective saturation concentration and the glass transition temperature parametrization of DeRieux et al., (2018) are considered. ~~simulated evapograms where particle viscosity is calculated using the VTF equation and glass transition temperature T$_g$ according to DeRieux et al., (2018) (black dashed line) or T$_g$ is calculated according DeRieux et al., (2018) and 30 K is subtracted from the T$_g$ value (grey dashed line).~~